THE UNIVERSITY OF
WARWICK

NAME: **Christopher Packer**

YEAR: **Year 4** INTAKE YEAR**: 2012**

TYPE OF PROJECT: **CH401/410 Research Project**

TITLE: **Controlling Ice Nucleation using Functionalised Graphene Oxide**

SUPERVISOR: **Prof. Matthew I. Gibson**

NUMBER OF WORDS: **8886**

ABSTRACT

Ice nuclei are particles that can catalyse the formation of ice crystals within a body of water. Their mechanism of action has long been the subject of investigation, but the role of structure and the properties of potent nuclei are still not fully understood. Graphene oxide has been examined for use in the control of ice nucleation along with an array of synthetic polymers. Nanocomposites of graphene oxide and polymers or thiols can be synthesised using a 'grafting to' method, with the aim of enhancing the ice nucleating properties of each of the individual components.

RAFT synthesised pNIPAM and a range of thiols, varying in hydrophilicity, were used to create unique nuclei that haven't been analysed for their ice nucleating ability before. An ice nucleation assay was performed on each sample to assess their activity and compare to known nuclei.

The resultant data exhibited the potential for graphene oxide based molecules as ice nucleation promoters, due to the temperature of freezing recorded being higher than has been seen in some previous studies.

ACKNOWLEDGEMENTS

I would like to thank Prof. Matthew Gibson for providing me with an enjoyable project, as well as answering all of my questions with great enthusiasm and optimism.

I would also like to thank the whole of the Gibson and Davies groups for their support with specific thanks to:

Sang-Ho Won for everything polymer related.

Ben Martyn for helping in all areas and taking his time to show me the lab techniques I required.

Henry Lee for helping me with TGA analysis.

Dr. Caroline Biggs for her knowledge of ice and analytical techniques.

ABBREVIATIONS AND SYMBOLS

°C	Degrees Celsius
%	Percentage
δ	Chemical Shift
μL	Microlitre
Acn	Acetonitrile
ACVA	4,4'-Azobis(4-cyanovaleric acid)
AFPs	Antifreeze Proteins
CTA	Chain Transfer Agent
DDT	Dodecanethiol
DMF	Dimethylformamide
DMP	2-(dodecylthiocarbonothioylthio)-2-methylpropanoic acid
DP	Degree of Polymerisation
GO	Graphene Oxide
HT	Hexanethiol
INA	Ice Nucleating Activity/Ability
IR	Infrared Spectroscopy
IRI	Ice Recrystallization Inhibition
M	Monomer
M_n	Number Average Molecular Weight
M_w	Weight Average Molecular Weight
NIPAM	*N*-Isopropylacrylamide
NMR	Nuclear Magnetic Resonance
OcDT	Octadecanethiol
pNIPAM	Poly(*N*-Isopropylacrylamide)
ps	Picoseconds
RAFT	Reversible Addition-Fragmentation Chain Transfer
SEC	Size Exclusion Chromatography
TGA	Thermogravimetric Analysis

LIST OF FIGURES

LIST OF SCHEMES

LIST OF TABLES AND EQUATIONS

SUPPORTING INFORMATION

Table of Contents

1. INTRODUCTION

1.1 CRYOPRESERVATION

Regenerative medicine aims to replace or repair damaged human cells and tissues to restore full functionality.[1] With a focus on the research into the growth of tissues and embryology, the treatment and storage of stem cells and embryonic cells is of very high interest. Mesenchymal stem cells (MSC's) are an effective bone marrow cell replacement and are a focal point in current research due to their ability to differentiate into a variety of cell phenotypes.[2] However, there is one main issue with MSC's and similar cells, and that is the low survival rates observed after cryopreservation,[3] a necessary step in the cells utilisation. This is just one example; any treatment using stem cells will require storage and transportation of cells. As a result, there is a need to investigate and understand the mechanism of cryopreservation in an attempt to optimise the process and increase cell survival.

Cryopreservation uses sub-zero temperatures to maintain the structure and activity of living cells and tissues.[4] The formation of ice is an inevitable consequence of the cooling of biological systems, and it is ice recrystallization that has been identified as one of the leading processes resulting in the death of cells during preservation.[5] The most notable mechanism of cell death during freezing is that the ice crystals formed simply pierce and tear into the cell membrane.[4] For that reason, any method of inhibiting the recrystallization of ice can significantly increase the viability of cells after freezing. Cryoprotectants are used to protect the cells from damage by preventing the amount of ice that can be formed, in and out of the cell – for use inside cells the protectant is required to have low levels of toxicity[6] to avoid additional damage.

Aside from ice recrystallisation inhibition (IRI), ice nucleation (the catalysis of ice crystals forming) is a vital, uncontrolled factor that can be used to control the viability of a cell.[7] Biological cells will undergo supercooling during cryopreservation, a process in which the cell will reach a temperature below its freezing point before nucleation occurs.[7] This exposes the cell to temperatures that aren't necessary for preservation and cause cell inactivation,[8] thus highlighting a need to control the temperature at which the system will freeze.

The importance of achieving an understanding of ice nucleation is largely related to knowing the mechanistic links between nucleation, ice nucleation inhibition, and antifreeze proteins. The simultaneous study of each component is key to being able to optimise an individual process and consequently optimising cryopreservation.

1.2 ANTIFREEZE PROTEINS

Antifreeze proteins (AFPs) were discovered in the blood of Arctic and Antarctic fish (Figure 1), allowing for them to survive the sub-zero temperatures[9] and they have been found naturally in some insects and plants since.[10] They act as cryoprotectants[11] as they can lower the freezing point of a substance (Thermal hysteresis) and have the effects of ice recrystallisation inhibition (IRI), and dynamic ice shaping.[12] It is thought that AFPs prevent the growth of ice crystals by inhibiting adsorption after binding to the surface of ice at the start of the freezing process.[13,14] AFPs have a complex structure and there is no exact template for a structure that will guarantee antifreeze activity as the natural proteins show a high level of diversity.[12] However, the AFPs found in the polar fish do show some similarity in structure with a common alanine-alanine-threonine tripeptide sequence with a β-D-galactosyl-(1-3)-α-D-N-acetylgalactosamine complex disaccharide attached to the threonine residue.[15] This structure provides a basis for synthetic AFP's with a focus on optimising thermal hysteresis as the aforementioned antifreeze effects are independent; meaning that different structures will promote one effect more than the others.[12]

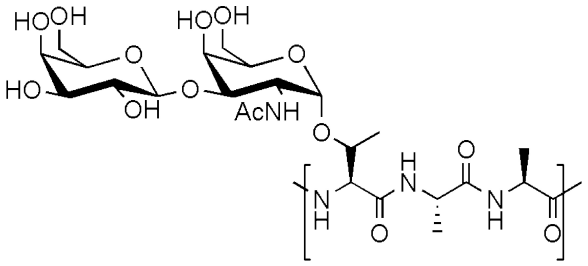

Figure 1 Antifreeze glycoprotein structure discovered in Arctic and Antarctic fish.[12]

1.3 ICE NUCLEATION

Ice formation is a very common process in nature as well as being one of the most important. Despite this, a large amount of the physiochemistry involved remains unknown. What is known, however, is that the formation of ice happens most

frequently at the surface of a material[16] and that impurities in water can provide nucleation sites that allow for ice to form at a higher temperature than expected.[17] Ultra pure water would be expected to freeze at -38 °C (there are slight variations in temperature due to the size of the droplet examined),[18] whereas sub-zero freezing temperatures in the range of -10 to -25 °C have been observed for impure water, which are likely to contain ice nuclei, even though the freezing point of water is defined as 0 °C. Ice nucleation can be heterogeneous or homogenous, where heterogeneous nucleation is the formation of ice when catalysed by a substrate in contact with the water, and homogeneous nucleation occurs without the presence of a nuclei, where the sample will reach approximately -38 °C and freeze due to changes in density.[7] An ice nuclei can be considered to be any molecule that once dispersed in water will increase the temperature and rate at which the droplet freezes as calculated by classical nucleation theory.[19] There are many applications, in addition to cryopreservation that rely on the understanding of ice, for example; atmospheric science, cryomedicine, cryosurgery, freeze-drying of pharmaceuticals, and food science,[16,18] which all add to the significance of the research in the field.

1.4 Ice Nucleation Inhibitors

The mechanism of AFPs discussed bypass the initial step of ice nucleation. It has been found that some AFPs can in fact inhibit this nucleation stage via adsorption to the ice nuclei or to dust particles.[20] In addition to AFPs,[21] polymers such as poly(vinyl alcohol) (PVA), polyglycerol, and poly(vinylpyrrolidone) (PVP), have all been reported to inhibit a variety of defined ice nuclei.[21–23] These polymers provide a new point of view for designing inhibitors and synthetic AFPs, therefore highlighting the need for a further understanding of the initial ice nucleation process, for example, analysing what makes an efficient ice nucleation promoter.

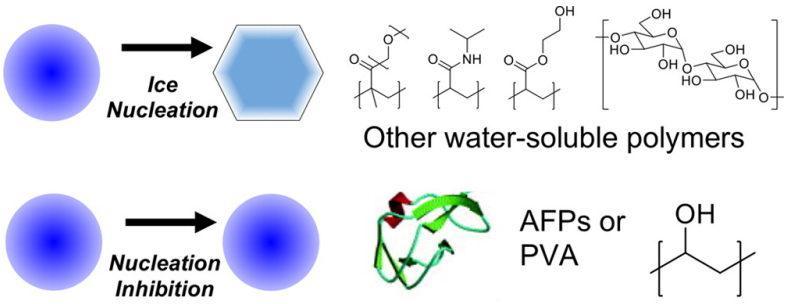

Figure 2 Demonstration of Ice Nucleation and Nucleation Inhibition with some notable molecules potent for each activity.[23]

1.5 Ice Nucleation Promoters (Ice Nuclei)

Similarly to AFPs there is as yet, no definitive guideline as to what constitute prolific ice nuclei, as it is still unknown exactly which type of compounds are capable of catalysing the freezing of water. Oxidised polymers (Figure 2) and carbohydrates[24] are thought to be involved with respect to cloud formation analysis, where such research also discusses the ice nucleating properties of molecules such as kaolinite and feldspar,[23] which are recognised nuclei present in the atmosphere directly involved in the formation of rain and clouds. Kaolinite and feldspar are mineral dusts, an important class of ice nuclei,[25] which originate from arid regions and are regularly transported thousands of miles from their source, for instance via Saharan dust clouds. The ice nucleation potential of each individual mineral within the dust cloud is poorly characterized at this current time.[26] Feldspar is one mineral within the dust clouds that is known to have ice nucleating potential and has been analysed[27] to try and determine its characteristics. It is globally distributed (Figure 3) and is considered to account for the majority of the ice nuclei that can be found in the atmosphere (despite only making up approximately 8% of the dust cloud),[27] that contribute to water freezing at temperatures around -15 °C. Thus explaining how, as described by classical nucleation theory, regular formation of clouds and rain can occur in the atmosphere at temperatures far higher than the expected.[19,26] Kaolinite is a clay mineral that accounts for approximately 13%[27] of the dust cloud and behaves similarly to feldspar, with respect to ice nucleation ability. It has been discovered that the higher the concentration of kaolinite in the sample, the higher the observed temperature at which it will freeze.[25] This can be linked to an increase in the total surface area of ice nuclei in the water, an important factor to consider when attempting synthesizing molecules with ice nucleation ability.

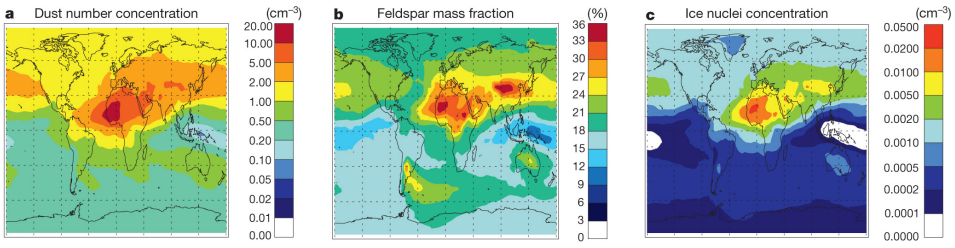

Figure 3 Global distributions of Feldspar and mineral dust ice nuclei.[27] a) Modelled dust number concentrations. b) Total feldspar mass fraction of dust cloud. c) Ice nuclei concentration due to K-feldspar.

The nucleation mechanism can follow one of the following freezing methods: deposition nucleation, condensation freezing, immersion freezing or contact freezing.[25,26] Deposition nucleation occurs in the vapour phase, with adsorption to the surface of the nuclei catalysing the freezing stage; condensation freezing involves vapour condensing onto the solid, before freezing; immersion freezing has a solid particle immersed in water allowing nucleation from within the droplet; contact freezing occurs upon collision of a solid particle with the water droplet causing nucleation from the surface of the droplet. The method of immersion freezing is most common for ice nucleating particles.[25,26]

Known inorganic ice nuclei tend to be large in size, relative to water molecules, and are often hydrophilic.[18] The most widely regarded properties valuable to ice nuclei are considered to be its hydrophobicity and whether the structure matches that of ice.[16] The water molecules ability to form bonds with the surface of the nucleating molecules shows a stronger adsorption that results in more efficient nucleation. A crystallographic match is supposedly able to allow for a stronger water-surface interaction as well as a hexagonal structure, mimicking the most stable and abundant hexagonal structure of ice, thus allowing the match to act as a template from which ice can form.[28] However, these properties are not definitive, as both, in some cases, have been shown to inhibit as well as promote ice nucleation.[29] Lupi et al[29] have shown, through experimenting with graphitic surfaces, that a change in hydrophilicity for rougher surfaces does not make a difference to its ice nucleation ability. Equally with the crystallographic match, it is assumed ice-like structures would be suitable for promoting nucleation but there are cases in which crystallographic matches have shown very little nucleation activity due to atmospheric water also showing an abundance of its cubic formation.[30] These factors contribute to the idea that we still know very little about ice nucleation and that there are numerous properties to consider.

One type of nuclei that does provide strong evidence for the idea of matching the lattice structure of water to catalyse ice formation is silver iodide (AgI). AgI is an inorganic ice nuclei[31] that has been used for cloud seeding, a form of weather modification. Its hexagonal lattice structure has a high similarity to that of an ice crystal. It is predominantly hydrophobic but does have hydrophilic pockets (approximately 25% of the lattice)[32] which are thought to be responsible for the initial interaction with water molecules. The initial step of the nucleation mechanism is for the water molecules to

rapidly (~3 ps) adsorb to the surface of the AgI lattice.[33] From here, ice starts to grow upon this initial layer, increasing in size over time.

Aside from minerals, ranges of natural and synthetic molecules have been discovered to have some ice nucleation potential. Biological particles from pollen, water fungi, and small particles of PVA have all shown nucleating ability.[18] PVA has also shown inhibition of ice growth and nucleation,[23] however the research gives a suggestion that synthetic polymers can have the necessary interaction with ice that are required for promoting nucleation. Furthermore, carbon based nanomaterials including; carboxylated carbon nanoflakes, graphene oxide (GO), oxidized single walled carbon nanotubes and oxidized multiwall carbon nanotubes, have all shown that they can be used as ice nuclei.[18]

1.6 Graphene Oxide

Graphene and its derivative materials, graphene oxide (GO) in particular, have proven to be very important and popular for research in recent years due to their versatility in structure and potential for a large variety of properties and therefore potential applications.[34] Graphene sheets are single atomic layers of carbon that are arranged in a hexagonal lattice. The monolayer itself is ideal for use in electronics due to its high carrier mobility and lack of a band gap.[35] One particular property of graphene-based products in relation to ice nucleation is their large theoretical surface area.[18] GO maintains this large surface area as seen with graphene sheets, but differs considerably structurally and practically, as well as being possible to produce it on a large scale.[36] An array of oxygen-based functional groups disturbs the carbon structure and introduces a degree of sp^3 hybridization to the structure. There is a lot of ambiguity with regard to the exact structure of GO and is therefore often described as being a family of materials.[37] A suggested structure is shown in Figure 4, which is based on the Lerf-Klinowski model. Carboxylic and carbonyl functional groups can be found on the edges of the sheet with hydroxyl and epoxy groups present on the basal plane.[38] These functional groups provide a hydrophilic property that allows for dispersion in aqueous solutions.[39] This ability to be dispersed makes GO suitable for functionalization (with polymers, nanoparticles, etc.), transportation, and deposition.

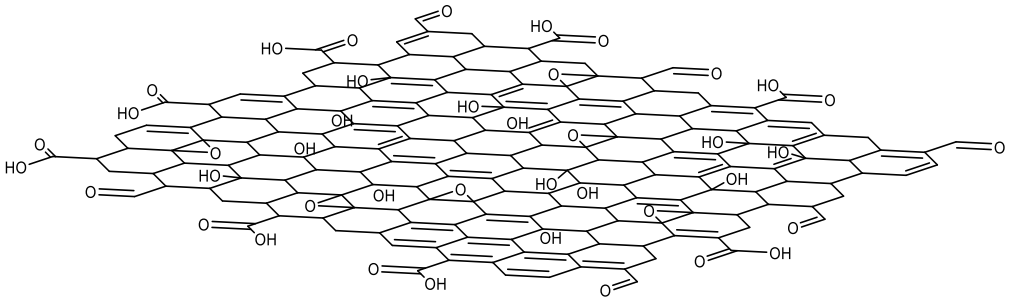

Figure 4 Lerf-Klinowski model of graphene oxide.

TEM has been used to show that the hexagonal structure of graphene is retained during transformation to GO.[35] GO can be considered to be more versatile than graphene due to its ability to be functionalized through the hydroxyl and epoxy functional groups, and can therefore be adapted for a variety of differing applications including drug delivery, medical imaging and cancer therapy.[40]

1.7 NANOCOMPOSITES

Nanocomposites are a combination of materials (phases) where at least one of the phases has dimensions in the nanometre scale.[41] They usually consist of a bulk material or a surface with a nano-dimensional phase chemically bound to it. The phases can differ in properties to enhance the, or increase the number of, desired properties of one phase, with enhancements being emphasized in nanometre dimensions (compared to micron scale),[42] nanocomposites can show combinations of properties that can't be accessed with conventional composites.[41] The addition of polymers or nanoparticles to the surface of carbon based materials, such as carbon nanotubes and graphene oxide (GO), is one method of attaining these enhanced properties.[41,42]

Synthetic polymers have been successfully attached to the surface of GO through a grafting to methodology.[43] Pre-formed polymers are bound to the surface of the GO as opposed to trying to functionalise the sheet with a chain transfer agent or an initiator and attempting to grow the polymer on the surface. This can be accomplished by using polymers formed by Reversible Addition-Fragmentation Chain Transfer (RAFT) that contain a thiocarbonylthio component at one end of the polymer chain. This group can be converted into a thiol via cleavage at the terminal thiol allowing for attack at the epoxide groups on the basal plane.[43]

1.8 RAFT POLYMERISATION

RAFT polymerisation is a process with great commercial popularity due to its compatibility with various reaction conditions[44] whilst being able to provide the polymer with a desirable, reactive end group.[45] A chain transfer agent is incorporated into the reaction containing the monomer and initiator, its role is to rapidly interchange the radical species to prevent the termination of a chain (Scheme 1).[44] This means that each chain can grow equally leading to a narrow molecular weight distribution.

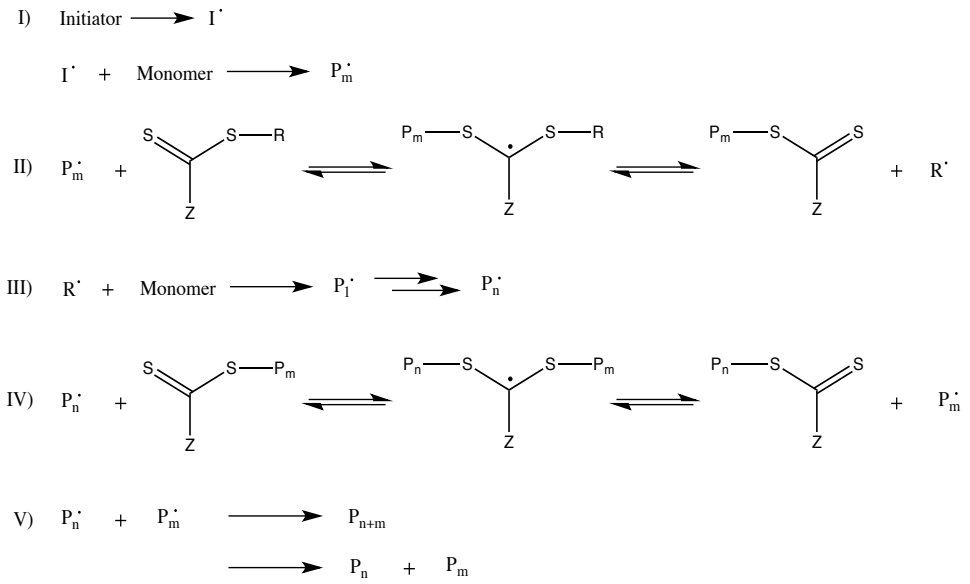

Scheme 1 General RAFT polymerisation reaction mechanism.

1.9 GOS ICE NUCLEATION ACTIVITY

All natural snow and ice, in its most stable form, shows a hexagonal structure.[46] GO shows a similar structure with its lattice of hexagonal carbon rings and as a result conforms to one of the professed properties of a good ice nuclei by displaying a crystallographic match. Moreover, the GO sheet is relatively flat and therefore will not disrupt the hydrogen bonding in the ice lattice as well as allowing for strong interactions between itself and the water molecules.[18] As well as the standard GO shown in Figure 1, GO that has been base refluxed has shown significant activity as the negative carboxylic groups are able to provide an anchor for nucleation followed by outward diffusion resulting in the growth of an ice crystal around the anchor site.[46] GO appears to exhibit many of the aforementioned properties desired for ice nuclei: large surface area, easily dispersed in water, and a hexagonal structure. Combined with the fact that it can be

modified for a selected application, GO is an ideal component to consider for synthetic ice nuclei.

2. Aims

With the optimum characteristics of an ice nuclei remaining unclear, the synthesis and application of potential nuclei can be used to suggest the theoretical properties. Graphene oxide has been shown to be extremely versatile whilst showing ice nucleation potential so could be an ideal base component for the molecule. As has been previously shown, thiols, and consequently thiol-capped polymers, can be grafted to the GO surface leading to the possibility of tuning the properties of the sheet to achieve a more efficient ice nucleation promoter. The functionalised GO sheets will aim to increase the temperature at which droplets of water will freeze.

The main targets of the project are:

i) Synthesize pNIPAM with a RAFT polymerisation technique ensuring that a thiocarbonylthioylthio end group is present.

ii) Graft synthetic polymers and a variety of thiols to the surface of graphene oxide.

iii) Examine the ice nucleation ability of each grafted graphene oxide sample via an ice nucleation assay involving freezing multiple droplet samples.

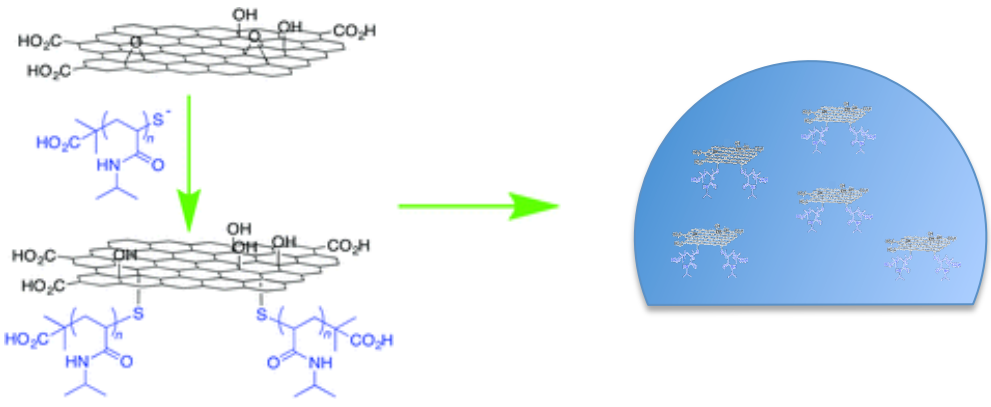

Figure 5 Graphical representation of the main aims of the project.

3. RESULTS AND DISCUSSION

3.1 POLYMER SYNTHESIS

Poly (*N*-isopropylacrylamide) (pNIPAM) is a thermoresponsive polymer that is soluble in water below 32 °C.[47] It is generally considered a hydrophilic polymer but above 32 °C, it becomes a hydrophobic molecule as this is above its lower critical solution temperature (LCST) and is therefore insoluble.[48] Its noted interactions with water make it a suitable polymer to try in ice nucleation analysis.

A RAFT polymerisation method was used, as it was important to ensure the presence of a thiocarbonylthioylthio end group[43] that could be activated for the ring opening of epoxides. The RAFT agent, 2-(dodecylthiocarbonothioylthio)-2-methylpropanoic acid (DMP) was ideal for this purpose and was therefore produced using the synthetic procedure shown in Scheme 2 (see S1 for NMR characterisation).

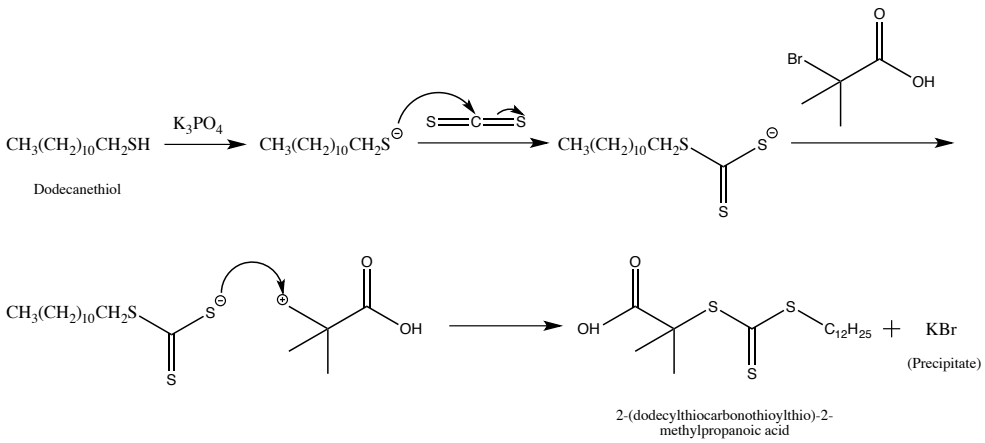

Scheme 2 Reaction mechanism for the formation of the DMP RAFT agent.

The successfully synthesized RAFT agent (Section (experimental)) was applied to the polymerisation of *N*-isopropylacrylamide (NIPAM) with two polymers being produced (Scheme 3) with differing degrees of polymerisation by modifying the ratio of monomer:chain transfer agent.

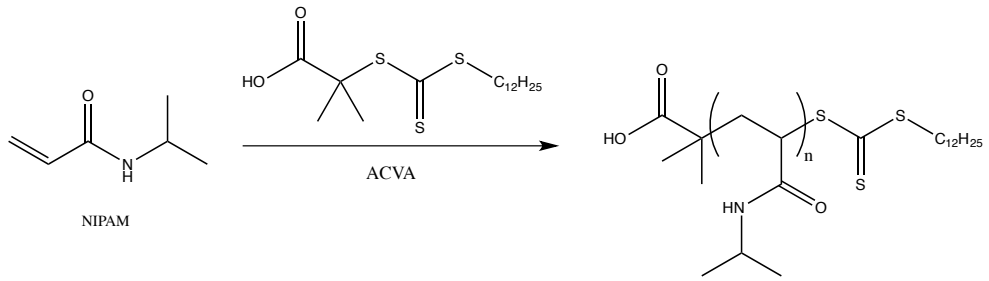

Scheme 3 Synthetic route for the polymerisation of NIPAM.

Size exclusion chromatography (SEC) data (Figure 6) confirmed the M_n and consequently the DP of each polymer. With the aim to synthesis two polymers of NIPAM that differ in DP in the interest of comparing the effect of polymer size on ice nucleation, one of DP 140 and one of 55 were produced, the ^{1}H NMR confirms their similarity in structure. The SEC data is summarized in Table 1.

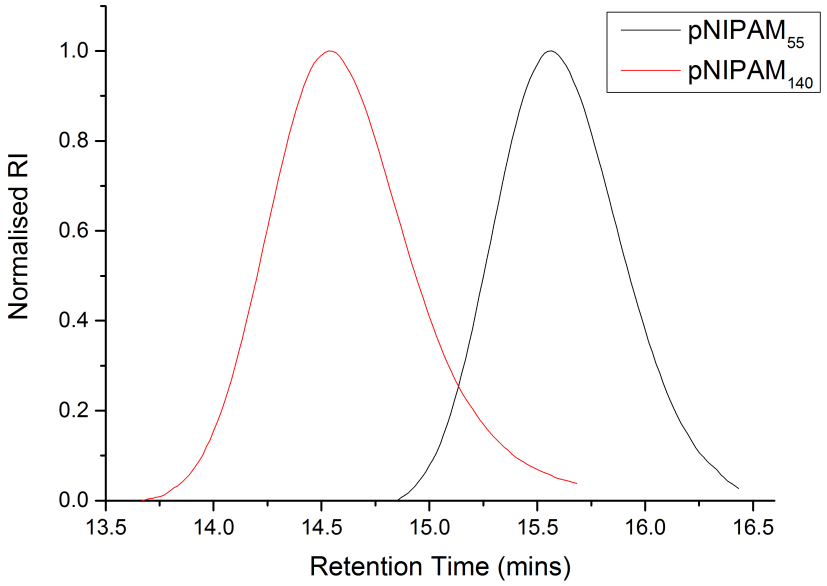

Figure 6 SEC analysis of the RAFT mediated polymers.

	Polymer	DP [a]	Conversion (%) [b]	Mn (SEC)	Mw (SEC)	Dispersity
1	pNIPAM	140	60.5	15700	17400	1.11
2	pNIPAM	55	85.0	6200	6700	1.08

Table 1 Summary of polymer analysis from SEC and NMR.

[a] calculated from SEC data. [b] determined from NMR using mesitylene as a reference.

The data shows that the polymers produced are well defined with each having a low polydispersity. The monomer conversion percentages given in Table 1 were obtained after the comparison of the relative peak intensities of the vinyl protons in the monomer and the mesitylene peak used as a standard, in the NMR analysis. Spectra (Figure 7) were recorded before and after polymerisation to provide the data for the consumption of the monomer during synthesis to be used in Equation 1.

$$Conversion = \frac{Integration\ of\ vinyl\ peak\ before - integration\ after\ polymerisation}{Integration\ of\ vinyl\ peak\ before\ polymerisation}$$

Equation 1 Calculating monomer conversion.

$$Conversion\ for\ pNIPAM140 = \frac{2.23 - 0.88}{2.23}$$

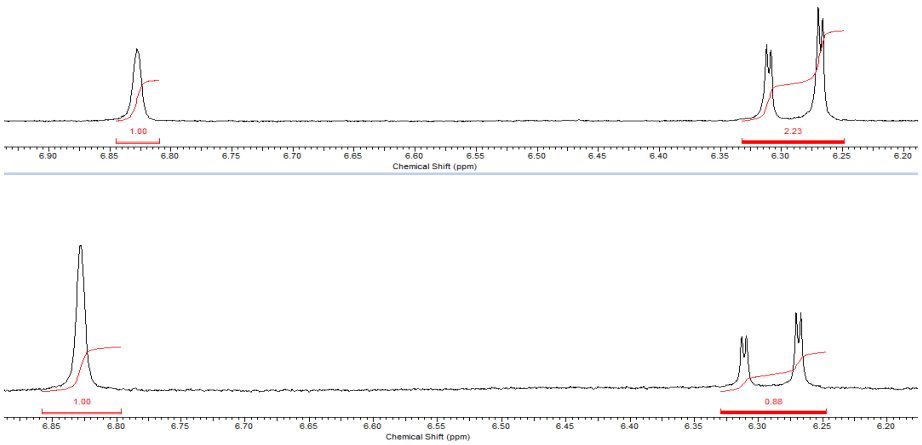

Figure 7 Example for $pNIPAM_{140}$ of the NMR of the reaction solution before and after polymerisation showing a decrease in the integration of the vinyl peaks from 2.23 to 0.88.

3.2 Grafting to the surface of Graphene Oxide

In addition to pNIPAM, a variety of thiols were chosen to graft to the surface of GO to show that thiols can successfully functionalize GO. Cysteine and dodecanethiol (Figure 8) were initially chosen to allow for the exploration of the effect of hydrophilicity with them being hydrophilic and hydrophobic, respectively. The GO sheets were functionalized via the ring opening of the epoxides on the basal plane (Scheme 4).

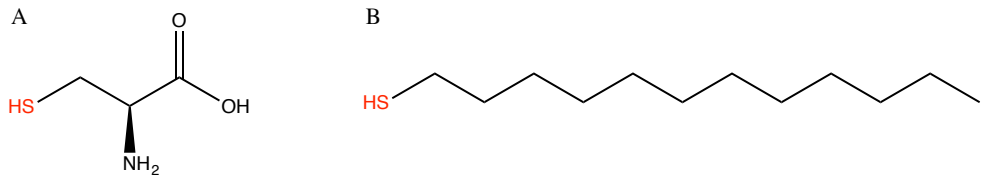

Figure 8 Structures of a) cysteine and b) dodecanethiol initially chosen to graft to the surface of GO. The thiol groups to be anchored to the surface of GO have been highlighted in red.

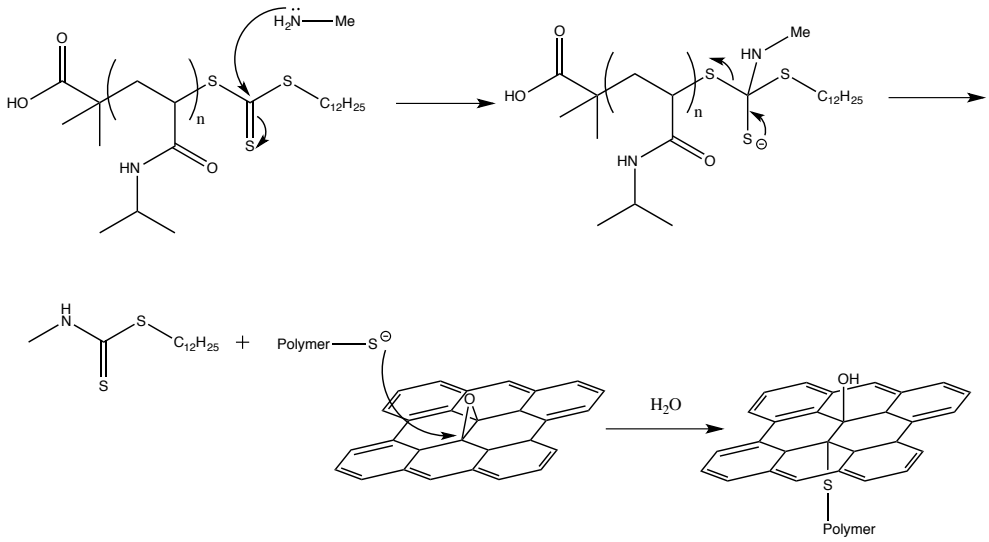

Scheme 4 Mechanism of epoxide ring open on GO via thiol attack. Showing the cleavage of the thiocarbonylthioylthio group to leave an active end.

The methods chosen for characterization of the grafted samples were thermogravimetric analysis (TGA); to provide information on thermal decomposition, and infrared spectroscopy; to monitor any changes in presence and/or abundance of key functional groups.

3.3 Thermogravimetric Analysis (TGA)

Previous studies suggest that the nanocomposites materials would show a major decomposition at a higher temperature than both GO and the isolated polymer or thiol.[43] The decomposition is thought to be due to the decomposition of the functional groups on the basal plane, edge, and vacancies in the structure, but this still needs clarification.[49] The stability, with regards to the epoxy groups on the surface, is vague[49] due to the random surface distribution,[50] so it can not be conclusive as to whether a

grafted polymer, or thiol, will indeed increase the thermal stability of the GO sheet. As a result, any deviation from the decomposition profile of GO observed in the profile of the functionalized GO (Figure 9), may show a form of modification.

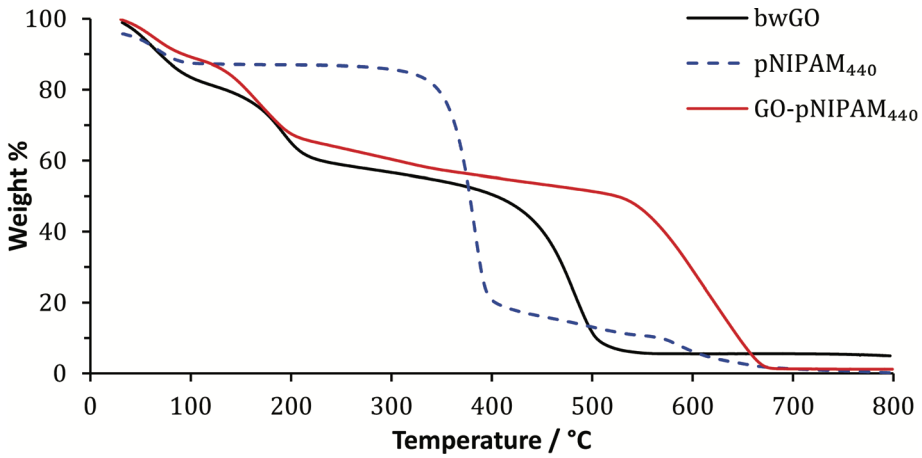

Figure 9 TGA data from previous work,[43] showing a change in decomposition profile of graphene oxide before and after functionalization with pNIPAM.

a)

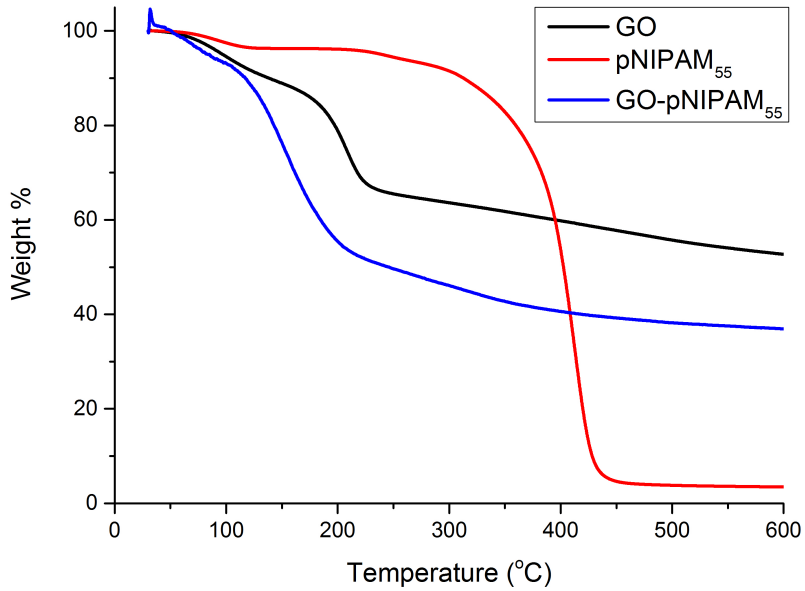

b)

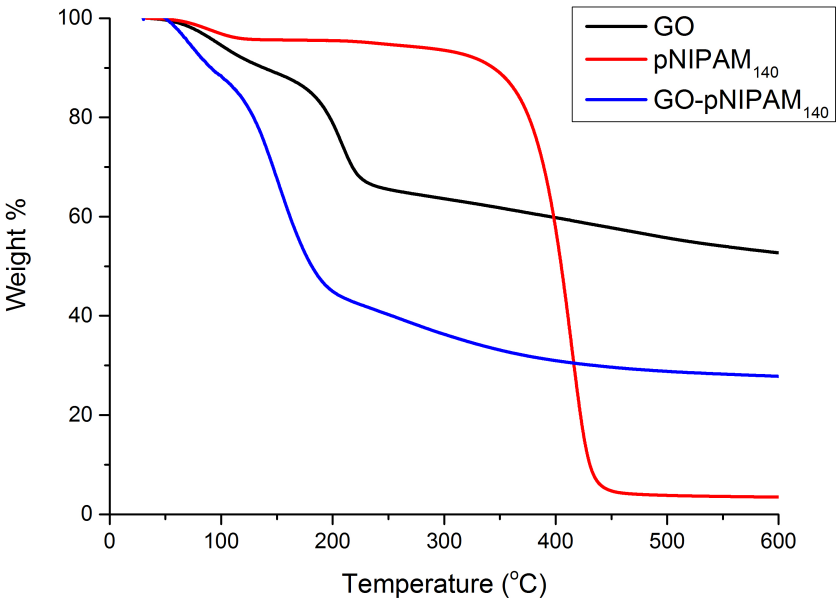

Figure 10 a) Decomposition profile of $pNIPAM_{55}$ grafted to GO and its isolated components, b) Decomposition profile of $pNIPAM_{140}$ grafted to GO.

Initial TGA data was recorded up to a temperature of 600 °C. The profiles of GO functionalised with the two pNIPAM samples (Figure 10), show a distinct change from that of GO. Supported by another obvious variation with the decomposition of the isolated polymer, it can be determined that the GO sheet has been modified in some form, and it is therefore likely that the polymer has been grafted to the surface. It may be expected that a large mass loss would be present around 400 °C due to the decomposition temperature of the NIPAM monomer, which is not the case for the GO-pNIPAM profiles. The fact that the mass loss isn't observed exposes changes to the stability of both GO and the polymer, with the potential for the thermal stability of the polymer being increased by anchoring to the carbon surface, leading to an expected mass loss beyond the 600 °C that has been measured. Similar evidence can be found with the comparison of the thiol grafted samples (cysteine and DDT) to the same GO profile (Figure 11).

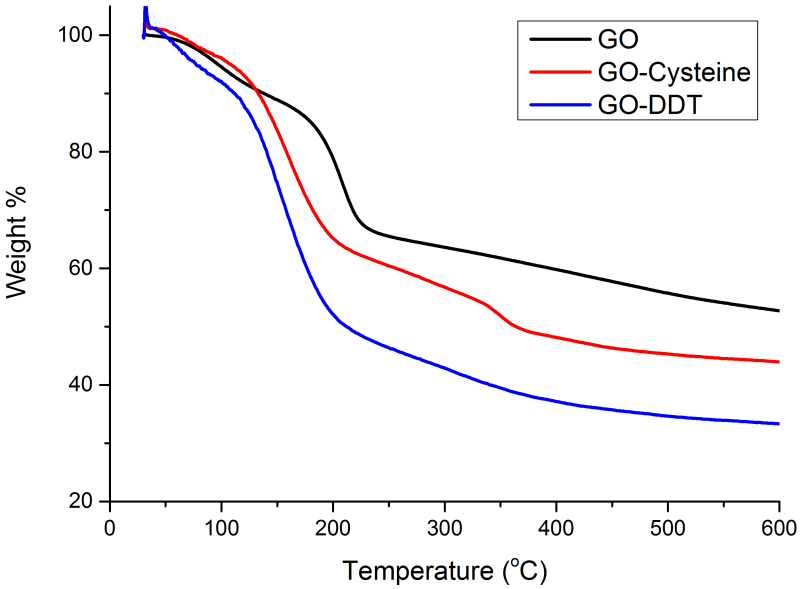

Figure 11 TGA data showing the trend in thermal decomposition of GO when cysteine and DDT are grafted to the surface.

The ice nucleation assay results for these samples, GO-pNIPAM compared to isolated pNIPAM in particular (see Section 3.5 and Figures 22-24), did not show too much of a change in ice nucleation ability (INA). The synthesis proved difficult in purification and isolation of the GO sheets, leading to the idea that there may still have been DMF, the solvent used, residing in the sample, hindering INA. It was decided that the synthesis was to be repeated, using $pNIPAM_{140}$ and DDT, with acetonitrile (Acn) as the solvent in an attempt to improve the purity of each sample and in turn observe an increase in nucleation temperature.

In addition to the change in solvent, the TGA data for the new samples was run to 1000 °C, as significant changes can be seen after 600 °C in Figure 9, and the profiles were not inspected up to 100% decomposition.

a)

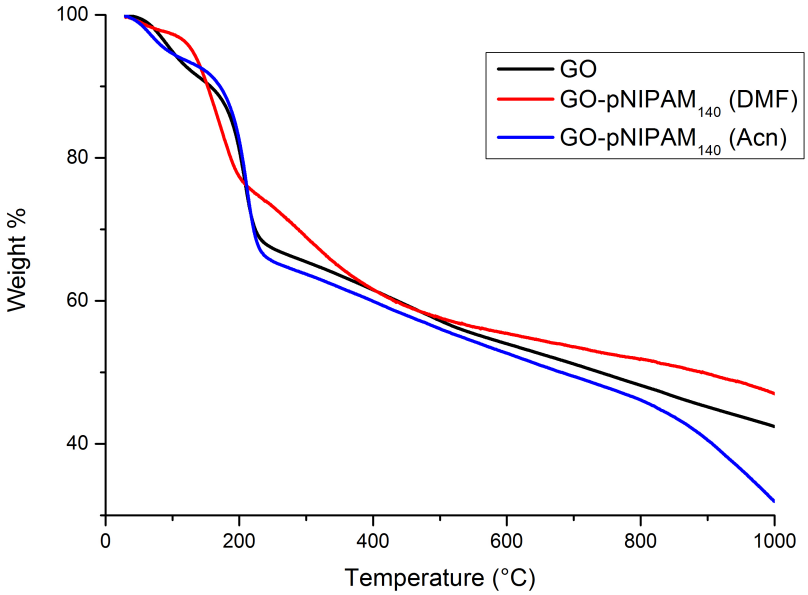

b)

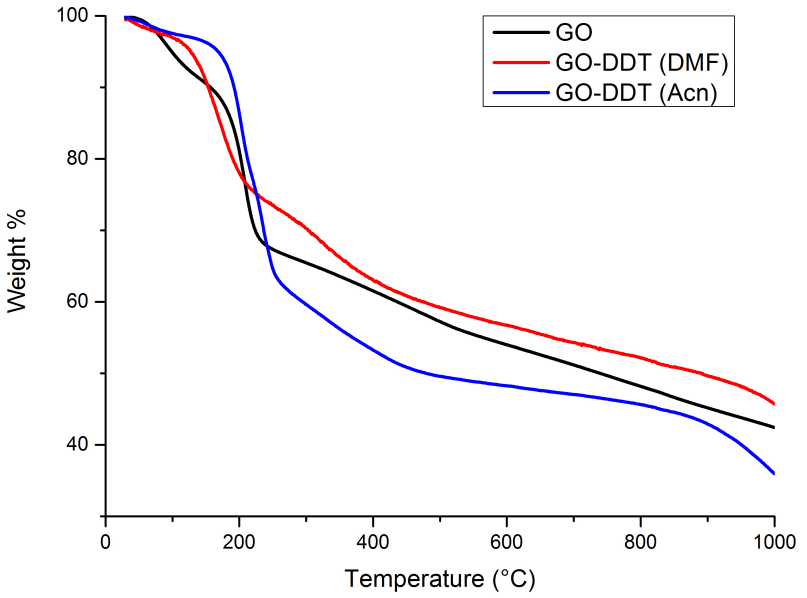

Figure 12 The decomposition profiles, as recorded by TGA, up to 1000 °C. Comparing each of $pNIPAM_{140}$ and DDT with the two differing solvents, DMF and Acn.

As can be seen for both of the Acn syntheses (Figure 12), there is an obvious change in mass beyond 600 °C. There is a hint of a change in mass loss occurring for the DMF syntheses but this can only be conclusive with analysis beyond 1000 °C. A distinct difference between the profiles of samples where DMF has been used in the syntheses and those using Acn is noticed. This is not to say that one of the GO based nuclei

hasn't been functionalized; as was previously discussed, the vagueness surrounding the stability of GO, with respect to the epoxide groups,[49,50] suggests that any variation in molecule or grafting density could either increase or decrease the thermal stability. This idea is highlighted in the thermal reduction of GO to graphene, where the nature and concentration of the oxidizing species, that bind to the surface, have a large impact on thermal stability and reduction efficiency.[50–52] The apparent large loss in mass at approximately 800 °C, could be due to the eventual loss of the grafted material that was not observed when the thermal decomposition was only measured up to 600 °C, or is the result of modifications made to the surface structure (epoxide groups converted to –OH groups) after the loss of the polymer or thiol causing the sheet to be more susceptible to decomposition.

After assessment of the INA of the new samples (see Section 3.5 and Figures 25 and 26), it appeared that the hydrophobic thiol provided a more efficient site of nucleation, on average across the two samples, when grafted to GO than pNIPAM. Consequently, a further two hydrophobic thiols were chosen to try and discover whether it is, in fact, the hydrophobicity of the molecule playing a part. Hexanethiol (HT) and octadecanethiol (OcDT) (Figure 13) allow for this investigation whilst providing information on the effect of size of the hydrophobic alkane chain, with a systematic comparison of alkane chain lengths of 6, 12, and 18 carbon atoms.

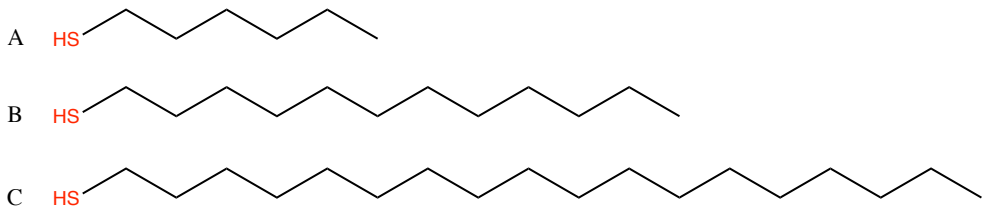

Figure 13 Structures of hexanethiol (A) and octadecanethiol (C) compared to the already grafted dodecanethiol (B). The thiol anchor group has been highlighted in red.

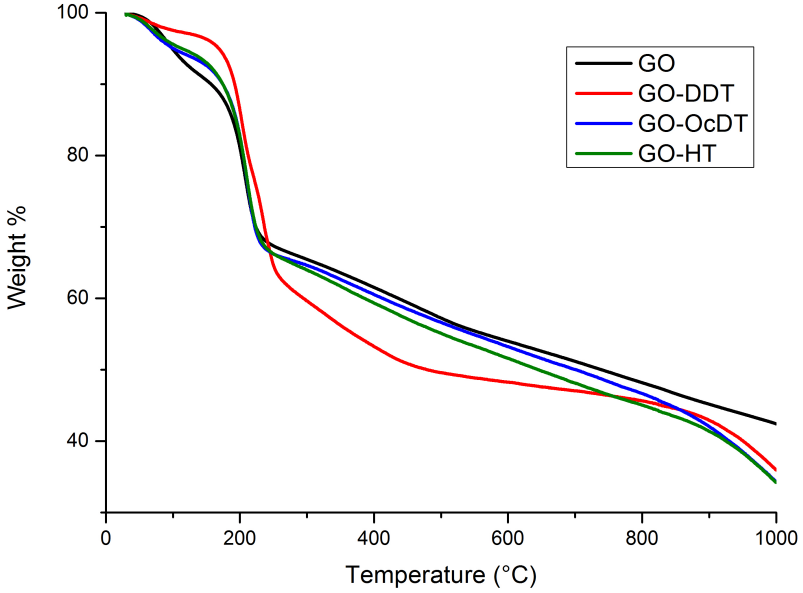

Figure 14 TGA analysis of hexanethiol, dodecanethiol, and octadecanethiol showing decomposition up to 1000 °C.

The final decomposition profiles (Figure 14) follow the same trend that can be seen throughout the samples. A similar shape with slight adjustments to initial rate of mass loss (with respect to increasing temperature), is likely to be caused by the gradual loss of anchor groups, with an increase in mass loss observed beyond 800 °C potentially due to the eventual decomposition of the GO sheet. Should this theory be correct, the TGA data shows that grafting to GO does alter the thermal stability of the sheet as no such change in rate of mass loss can be seen in the isolated GO profile.

3.4 Infrared Spectroscopy

Long acquisition IR (acquisition times of 1 hour) was required to provide spectra with well-defined peaks. Should the 'grafting to' method have been successful, the most obvious transformation in the spectra will be an increase in intensity of the broad –OH peak between 2500 cm^{-1} and 3700 cm^{-1} as a result of epoxide ring opening, adding to the stretch present from the alcohol and carboxylic acid groups decorated the edges of GO. Alterations in the –CH regions at 2850-3000 cm^{-1} and 1350-1480 cm^{-1} will be indicative of the presence of the alkane chain found in each of the hydrophobic thiols. However, these peaks may be difficult to distinguish depending on the length of alkane chain and grafting density; ultimately the number of –CH moieties present. Besides the –OH peak

change, the GO samples grafted with pNIPAM can be expected to show peaks transmitted at 1653, 1554 and 1381 cm^{-1} that are assigned to the C=O of the amide.[53]

a)

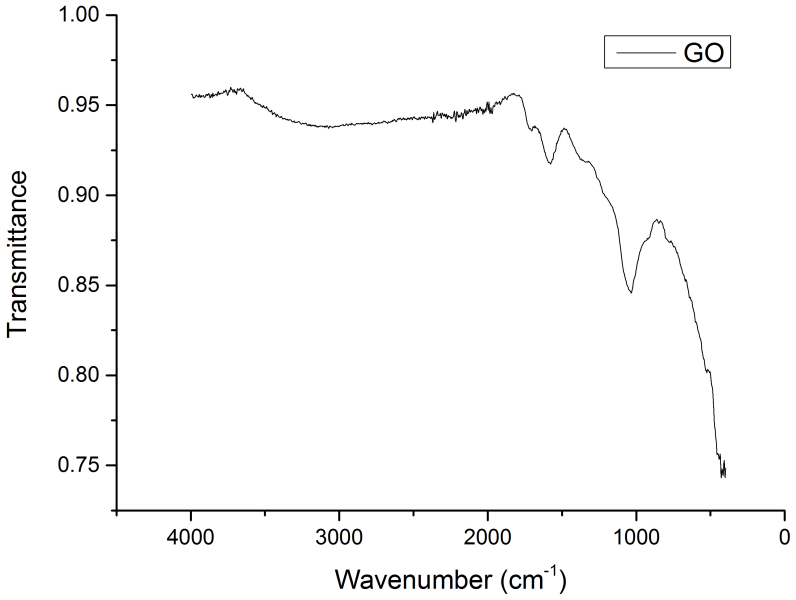

b)

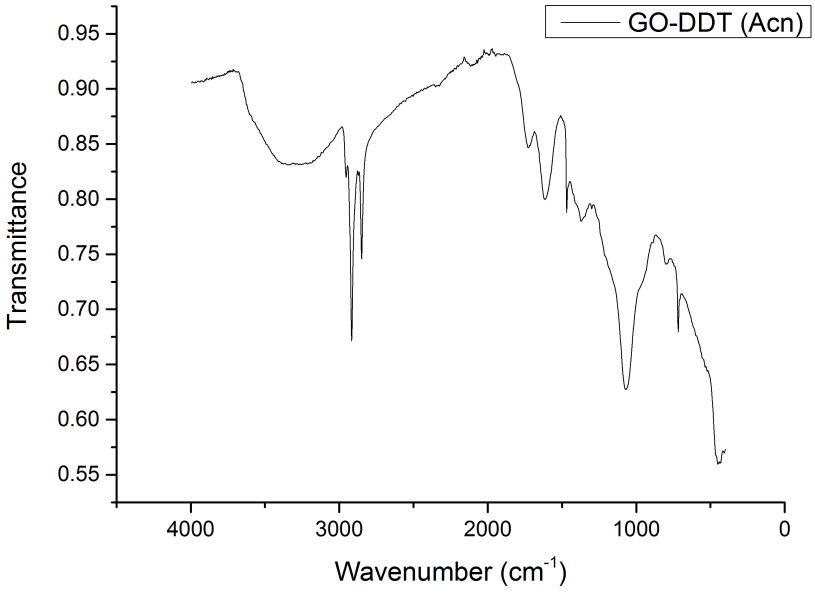

Figure 15 IR spectra of a) Isolated GO sheets b) GO functionalised with dodecanethiol using acetonitrile as the synthetic solvent – an example of the expected changes to the GO spectra with alkane thiols grafted to the surface.

The GO-DDT sample using Acn as a solvent (Figure 15) clearly displays each of the aforementioned alterations to the IR spectra expected of a functionalized GO sheet. An increase in intensity for the –OH peaks, sharp peaks around 2850-3000 cm^{-1}

representing the alkane CH's, and finally, an obvious change to the –CH region lower down the scale (1000-2000 cm^{-1}). The combination of the decomposition profile, showing modifications to the GO used, and the IR spectra, indicating that DDT is present as well as implying that the ring opening of epoxides has occurred, proposes that DDT has been grafted to the surface of GO.

IR spectra obtained for the grafting of pNIPAM to GO (Figure 16), also showed the expected signs both with the use of DMF and Acn as the solvent.

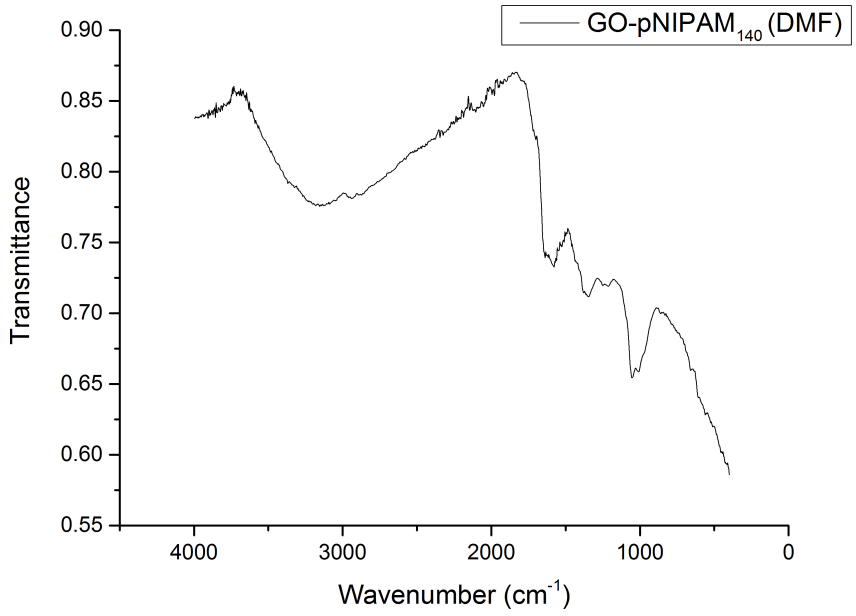

Figure 16 An example of the IR spectra recorded when pNIPAM was grafted to GO's surface.

Between 1500 and 1750 cm^{-1}, a new peak can be seen when compared to the spectra of GO, as is the case for the presence of an amide carbonyl. The discussed changes in –OH peak and –CH peaks are also noted in the spectra for GO-$pNIPAM_{55}$, and the other alkane thiols (see supplementary information).

The use of IR spectroscopy has enabled the detection of both pNIPAM and the alkane thiols to contribute to the evidence that the synthetic method used was successful.

3.5 Ice Nucleation Assays

An ice nucleation assay was used to assess the activity of the successfully functionalized GO samples. Milli Q water, GO on its own, and a sample of each of the

synthesized polymers were examined as well in order to create a comparison and deduce whether the grafted GO samples have a noticeable increase in nucleation activity.

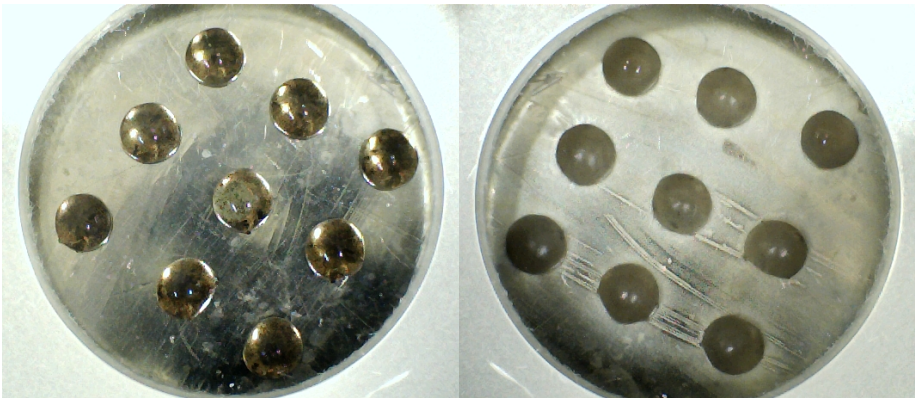

Figure 17 Example of how the droplets are displayed on the glass slide before (left) and after (right) the droplets have been subjected to freezing conditions.

Each individual assay consisted of freezing 8 or 9 droplets (1 μL) (Figure 17) with a minimum of 24 droplets of each sample tested in total. In order to measure individual droplets, a hydrophobic barrier was introduced on top of each slide to prevent the spreading of each sample across the surface. Water droplets will freeze in a stochastic nature, meaning that, the order of samples freezing will be unpredictable (Figure 18) and the temperature at which each drop freezes will vary in different tests. This means the distribution is not error in results but a natural variance in nucleation temperature. This leads to the need to test multiple drops in each assay, as a single data point is not useful, with the assay then repeated with fresh droplets of the sample.

Figure 18 A view of the nucleation progression of the samples freezing in a stochastic manner. Frozen droplets have been highlighted with a red circle.

The nucleation point of each droplet was recorded manually, and displayed as a percentage of total drops frozen in the following presentation of data.

Initially, tap water and Milli Q water were both assessed in order to show that the presence of impurities in water lead to ice nucleation as well as providing a base to compare the results of the GO based nuclei to.

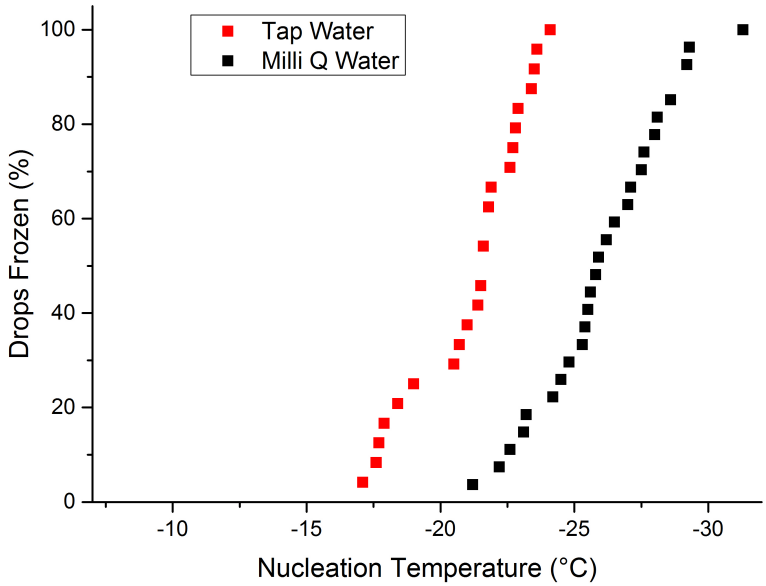

Figure 19 Freezing point distribution showing the nucleation temperatures of the samples of tap water and Milli Q water.

As can be seen from the nucleation distributions (Figure 19), the nucleation point of impure water is considerably higher than the ultrapure water, which tends more to the values shown in nucleation theory but won't reach the proposed values of -38 °C[7] as Milli Q water is still not 100% pure. Values fall between -20 °C and -35 °C, this has also been noted in previous experimentation,[54] which aids the approval of the analytical technique used as a method to attain quantifiable and comparable ice nucleation data.

GO alone is known to hold some nucleation activity[18,19,29] and so has been tested in the ice nucleation assay, suspended in Milli Q water to observe if it does act as a nuclei in this particular test, it will also further validate any potential nucleation ability of the grafted samples. The suspension or solution of the samples in Milli Q water represented in the assay distributions, are all of 2.5 mg/mL concentration unless stated otherwise.

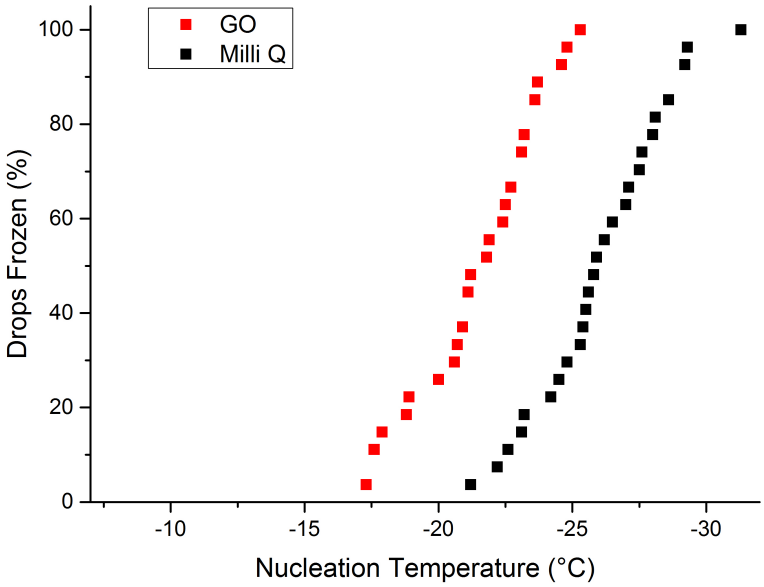

Figure 20 Ice nucleation distribution of graphene oxide compared to Milli Q water.

It was observed that GO did act as an ice nucleation promoter, showing similar values to tap water (Figure 20). In addition to the GO assay, the two synthetic polymers were also examined, each showing similar values to that of the tap water assay (Figure 21). This doesn't necessarily mean that pNIPAM can act as a nucleation promoter based on the evidence shown, the same can be said for the GO assay, but emphasizes the fact that impurities added into pure water will increases the temperature at which nucleation will be observed.

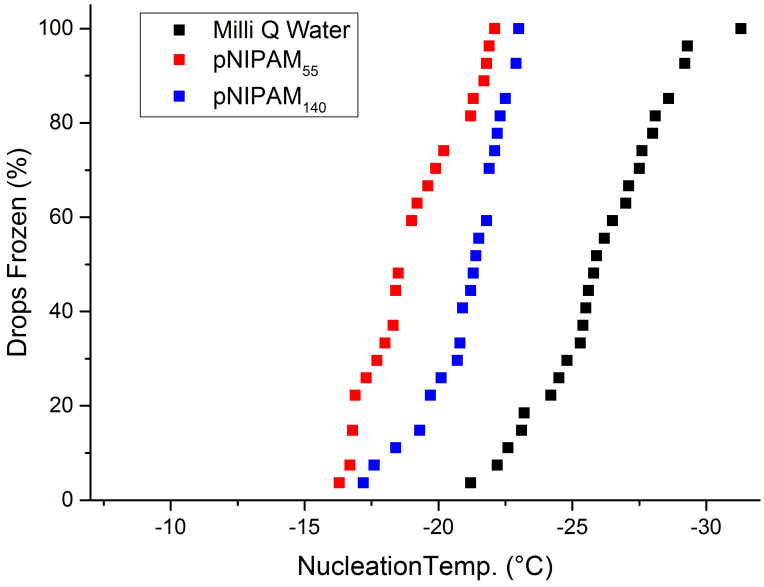

Figure 21 Ice nucleation distributions of both synthesized polymers before being used to functionalize GO.

The polymer-grafted samples of GO, using DMF as the solvent, were initially tested for ice nucleation ability, along with the cysteine and dodecanethiol (DDT) functionalized samples. The apparent improvement in nucleation ability of GO when cysteine and DDT were introduced (Figure 22) is of great interest as it suggests that there may not be difference between the usages of hydrophilic or hydrophobic groups that have been discussed in the literature. [28,55,56]

a)

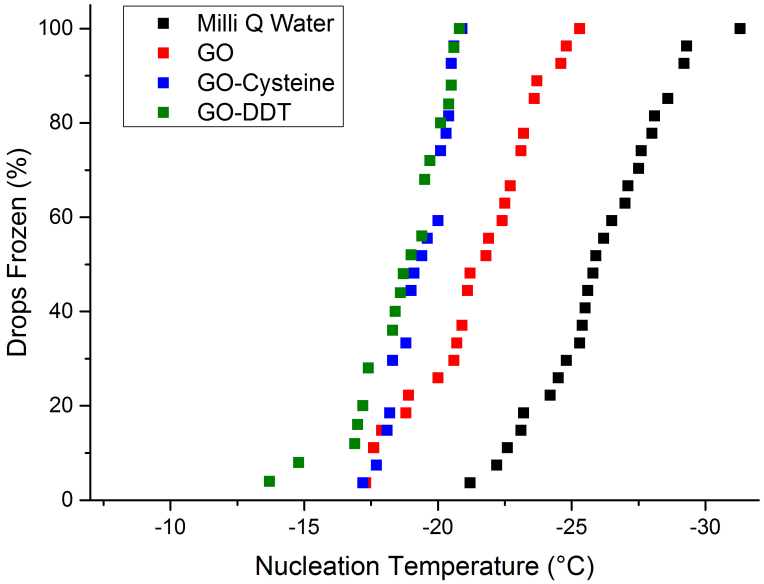

b)

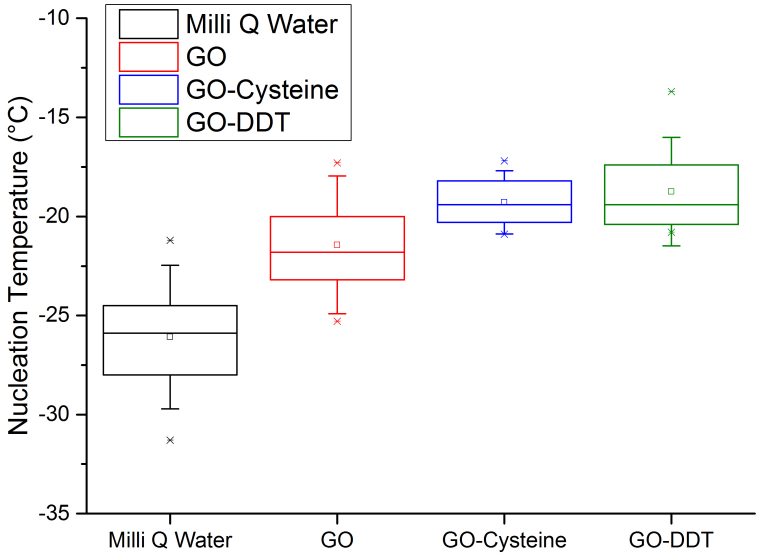

Figure 22 a) Ice nucleation distribution comparing the activity of cysteine and dodecanethiol once anchored to GO b) Box and whisker diagram comparing the ice nucleation ability of each nuclei, it displays the median (centre line), 25-75 percentiles (box), and the standard deviation (whiskers).

A box and whisker plot (Figure 22) has been chosen as a way of directly comparing the INA of each of the nuclei. The representation evidently shows the thiol modified GO to have an increased INA. It should be noted that the whiskers on the plots represent the standard deviation of the recorded nucleation temperatures, as this is more important than the upper and lower boundaries when considering the stochastic nature of water freezing.

Results for the polymer-grafted GO enforce an idea that the exfoliation of graphene oxide can improve its ice nucleating properties due to a noticeable difference in the freezing plots (Figure 23).

a)

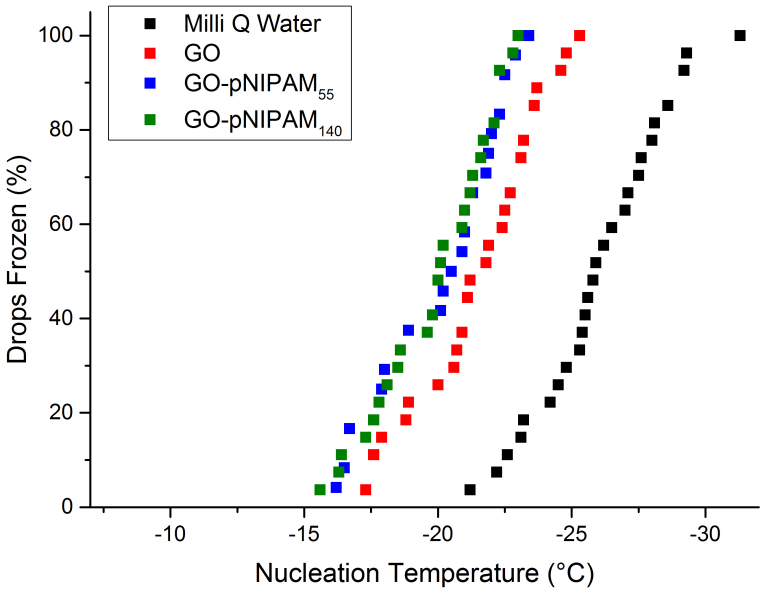

b)

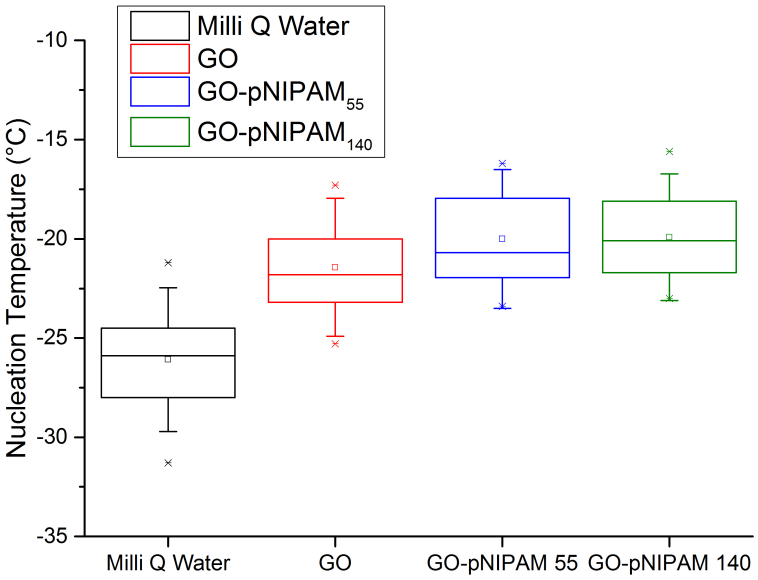

Figure 23 a) Ice nucleation distribution of GO-pNIPAM comparing both size polymers b) Box and whisker diagram comparing the nucleating ability of the grafted samples to GO and Milli Q water.

Again, the box and whisker plot (Figure 23) is able to show that the grafting of a polymer increases the INA as the box, consisting of the 25-75 percentiles, and the median (centre line), is at higher temperatures for both sizes of pNIPAM. When the distributions of the polymer samples, both grafted to GO and the polymer on its own (Figure 24), are compared, there is little notable difference in the nucleation temperatures. This observation, in conjugation with the noted difficulties in purification, resulted in the decision to try the synthesis using acetonitrile as the solvent.

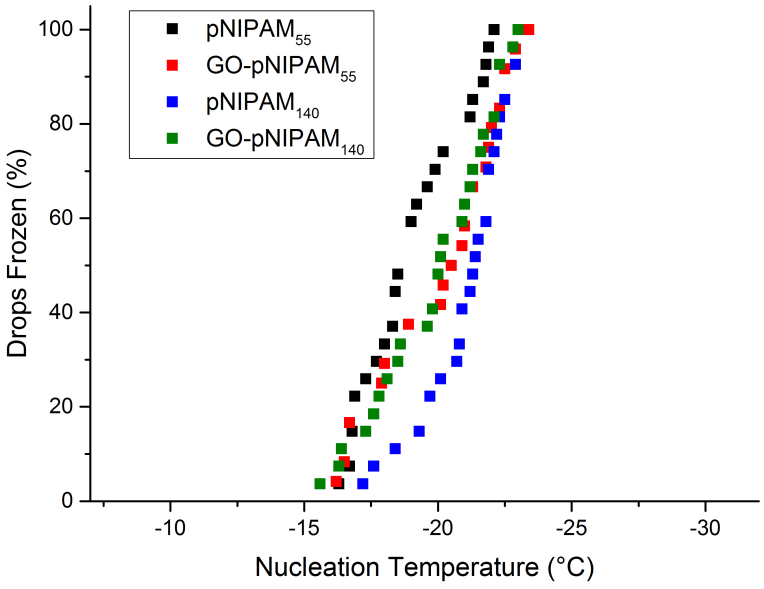

Figure 24 Ice nucleation distribution comparing the activity of pNIPAM before and after grafting to the surface of GO.

PNIPAM$_{140}$ and DDT were grafted to the GO flakes using Acn as the solvent, along with HT and OcDT, and were analysed to discover whether the change in synthetic solvent produces the anticipated improvement in INA.

a)

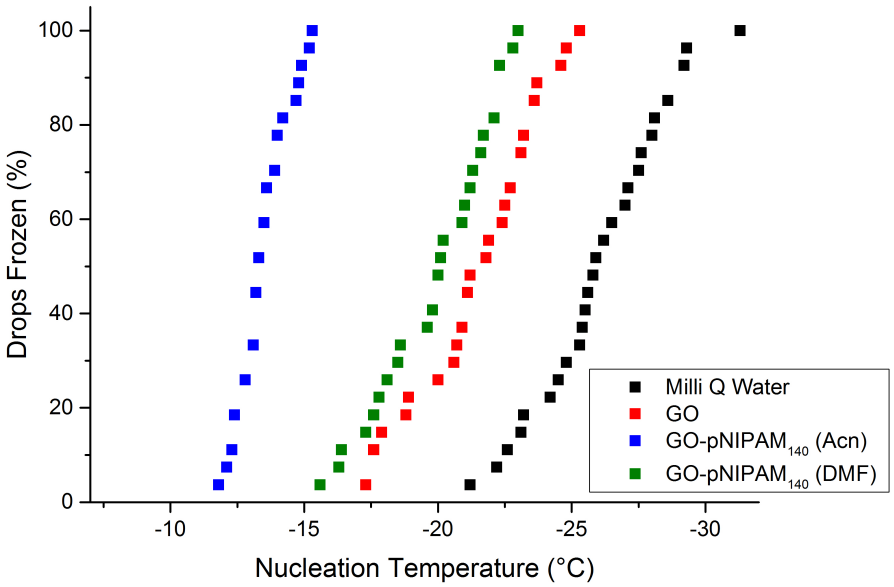

b)

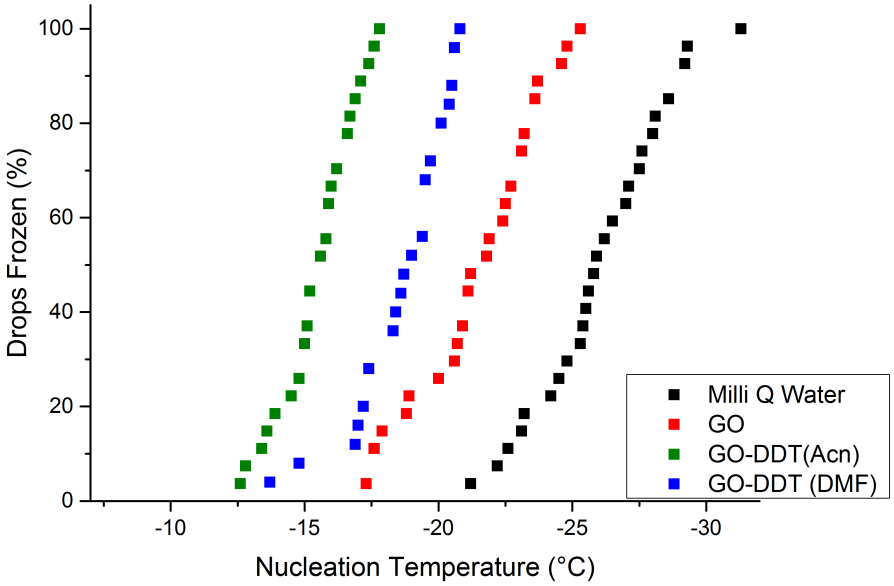

Figure 25 Ice nucleation distributions comparing the nuclei when DMF was used as the solvent in the synthesis and when acetonitrile was used a) GO-pNIPAM$_{140}$ b) GO-DDT.

The use of Acn did in fact optimize the nucleating potential of the synthetic molecules as is evident from the measured freezing points of the droplets (Figures 25) and is emphasized by the visual comparison of the box plots (Figure 26) with GO functionalized with pNIPAM$_{140}$ seemingly the strongest ice nucleation promoter so far.

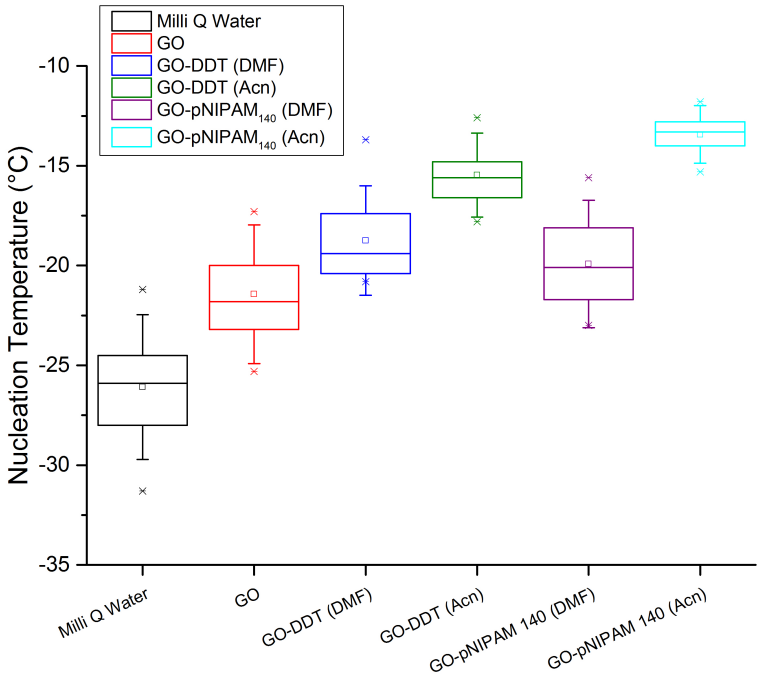

Figure 26 Box and whisker diagram displaying the effect of solvent use on the nucleation activity of the grafted GO nuclei.

A distinct difference in the nucleation distributions of the samples synthesised with acetonitrile as the solvent is somewhat surprising considering that the IR spectra (Section 3.4) and decomposition profiles (Figure 12) suggest that grafting has occurred for each case. However, the TGA data does suggest a difference in the stability of the GO sheet, which could mean a greater grafting efficiency when using Acn, resulting in an idea that the greater the grafting density the better the INA.

The final assays examining two more hydrophobic thiols, after DDT appeared to be the best nuclei from the initial nucleation distributions, show further improvement in catalysing the freezing of water.

a)

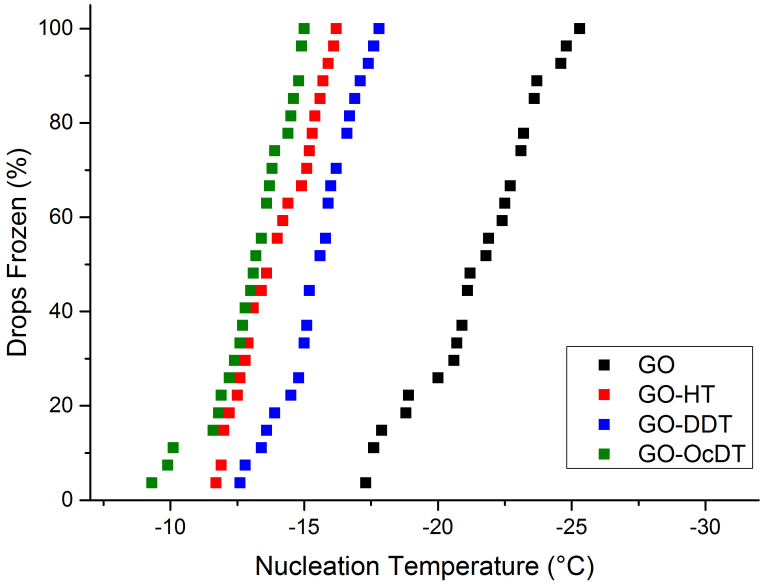

b)

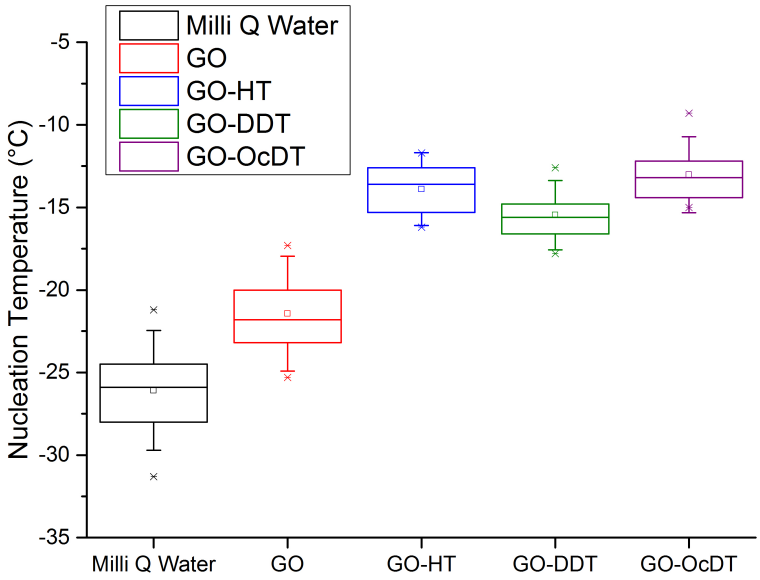

Figure 27 a) Ice nucleation distribution comparing any differences when the alkane thiol anchored to GO's surface is changed, using hexanethiol, dodecanethiol, and octadecanethiol. b) Box and whisker diagram showing the significant improvement in nucleating ability of the thiol grafted GO samples.

GO-HT and GO-OcDT show significant improvements on GO as can be seen in Figure 27, with OcDT functionalized GO showing little deviation below -15 °C. There isn't a distinct trend between the different chain length thiols but this does not confirm that the length of the grafted molecule doesn't play a part in ice nucleation. This is because the

grafting density has to be considered for a definitive answer but this cannot be determined from the analytical techniques discussed.

Each of the hydrophobic thiols has greatly improved the INA of GO and the results can be considered meaningful with respect to understanding the requirements for ice nuclei as the nucleation temperature values are considerably lower than has been recorded for a range of natural mineral dusts, using a similar assay (Figure 28).[27,57]

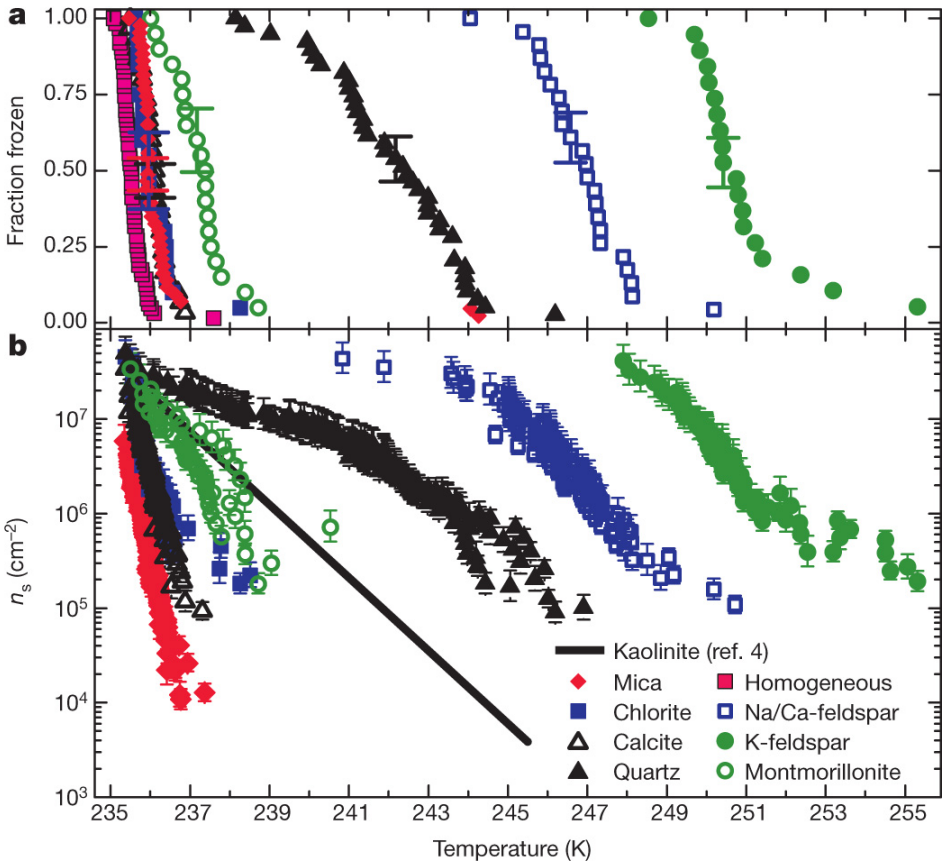

Figure 28 Experimental freezing results for individual minerals. a) Ice nucleation data for droplets (14-16 μL in diameter) containing the mineral dusts b) Nucleation site densities.[27]

The distributions for the minerals are all compared on a temperature scale ranging from approximately -39 °C to -17 °C. Each of the GO based nuclei discussed have shown the ability to nucleate the freezing of water at temperatures higher than for feldspar and kaolinite, for example, when comparing the methods. For this observation to be definitive each nuclei would be required to have been examined with exactly the same procedure, however, the sets of data of both assays can be used to validate the use and nucleating properties of functionalized grapheme oxide.

It has been proposed that the INA of nuclei will increase as its total surface area increases[58] and so the concentration of the GO based nuclei was increased from 2.5 mg/mL to 10mg/mL.

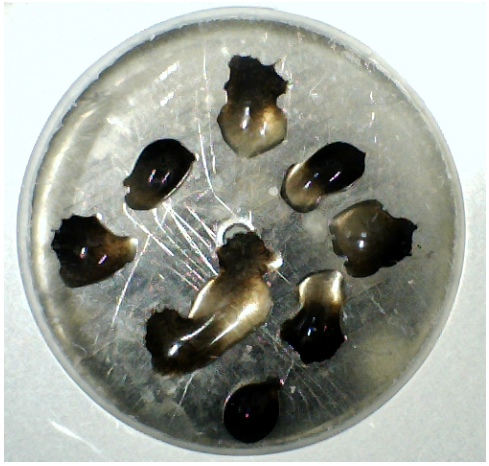

Figure 29 Droplets containing a GO sample at a concentration of 10 mg/mL where the droplets are unable to retain their shape for measurements.

Increasing the concentration to 10 mg/mL appeared to introduce a degree of instability to the droplet, as it no longer remained in a spherical shape atop of the hydrophobic barrier (Figure 29), and therefore the INA could not be assessed in an reliable manner. In general, concentrations exceeding 2.5 mg/mL become problematic to analyse with this particular method due to the black colour of the sample making it difficult to distinguish an ice droplet from a water droplet.

Ideally, for practical use in cryopreservation, the minimum amount of nuclei needed to encourage freezing should be used. The apparent strongest catalyst, GO-OcDT, was used to make samples at lower concentrations than previously measured, to push the limits of its nucleating abilities.

As can be deduced from the concentration dependent nucleation temperatures (Figure 30), a greater concentration of nuclei in the Milli Q water droplet has a greater chance of catalysing the freezing of the droplet due to the increase in total nuclei surface area. Despite this, the GO-OcDT nuclei are still potent promoters even at 0.1 mg/mL in a 1 µL droplet.

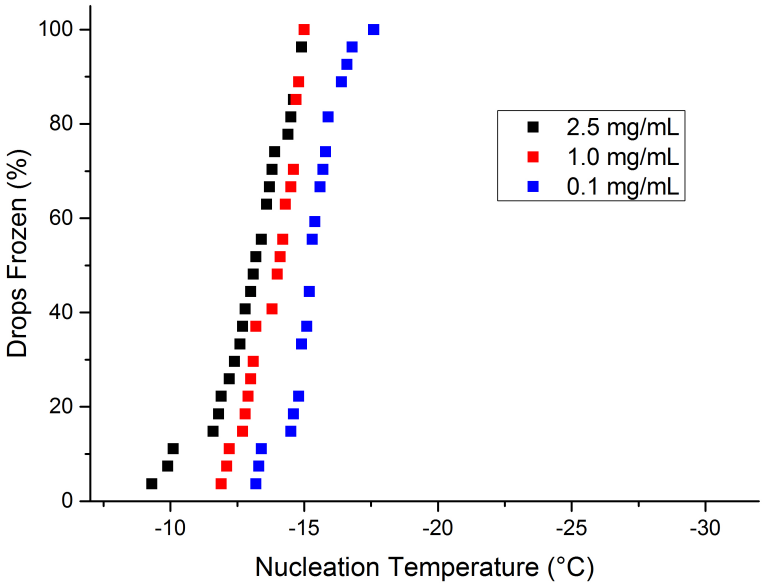

Figure 30 Concentration dependent ice nucleation distributions of GO-OcDT at 2.5, 1.0, and 0.1 mg/mL.

Even though the GO-OcDT nuclei is not as potent at lower concentrations, it is still a vast improvement on the nucleating ability of GO (Figure 31) and is one of the best nuclei reported to date.

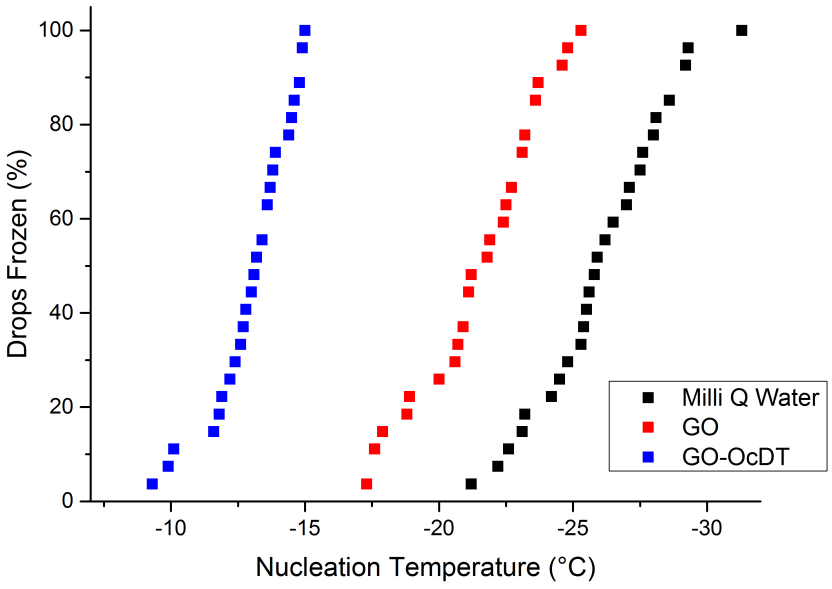

Figure 31 Ice nucleation distribution emphasising the impact of grafting OcDT to the surface of GO.

4. CONCLUSION

A RAFT agent was successfully synthesised and then used to mediate the polymerisation of two well-defined pNIPAM molecules that contained the desired thiocarbonothioylthio end group. This group was cleaved to leave a terminal active thiol, along with the activation of hydrophilic and hydrophobic thiols, which were all able to open the epoxide rings on the basal plane of GO so that they were grafted to the surface.

A change in solvent used during the grafting of the thiols to the GO surface was implemented and showed more positive results with regards to the INA of the functionalised GO molecules. This improvement can be attributed to the ease of purification and/or a more efficient grafting density.

The challenges arose with proving that the chosen thiols were present on the surface of GO. TGA and IR were both able to provide strong hints towards the effectiveness of the chosen 'grafting to' method. Furthermore, the ice nucleation assay itself can be considered as an extra method of determining the nature of the exfoliated GO sheets due to the observed differences in INA before and after modification.

No particular correlation was found when investigating the effects of alkane thiol chain length on ice nucleation but the longest chain molecule, GO-OcDT, provided a remarkable nucleation distribution.

Ultimately, all of the functionalised samples of GO showed a significant increase in ice nucleation ability to that of GO, with one exceptional modification. The success of the nuclei provide valuable data when considering the important properties of ice nuclei, and when used in conjugation with future research into carbon nanomaterials interacting with water, a greater understanding of the freezing behaviour of water can be achieved.

5. FUTURE WORK

The data recorded clearly showed the nucleating ability of GO modifications but does not conclude any effects that come as a result of changing the hydrophilicity. A greater range of thiols should be screened for INA with thioglycerol (Figure 32) an ideal hydrophilic thiol to investigate and compliment the conducted research on hydrophobic thiols.

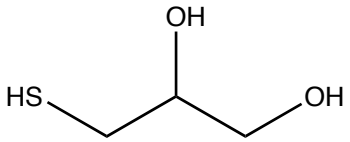

Figure 32 Molecular strcuture of thioglycerol.

Ice nucleation distributions for pNIPAM showed the potential of using polymers to functionalise GO but this was not further explored due to the potential seen in the hydrophobic thiols. As mentioned for thiols, a variety of RAFT mediated polymers should be examined to observe any differences between thiols and polymers anchored to the surface of GO or to reinforce the idea that the functionalisation of GO is the leading cause of ice nucleation promotion.

The manual recording of data proved to be a limitation within the investigation due to the fact that only a small number of droplets can be tested at one time. For conclusive data, a vastly greater number of nucleation points will be required for each sample, which is not feasible under the current method. A computerised method monitoring the state of each droplet will improve the rate that data is recorded, allowing for more extensive reports and a wider range of nuclei able to be tested.

Exfoliated GO is an ideal base to carry forward for future research into what the optimal properties and structure of ice nuclei really are.

6. EXPERIMENTAL

6.1 MATERIALS

All solvents and reagents were used as received from the supplier. The thiols used to graft to GO were bought from Sigma-Aldrich with the GO itself, supplied by Dr. Jon Rourke's research group at the University of Warwick.

6.2 ANALYTICAL METHODS

6.2.1 NUCLEAR MAGNETIC RESONANCE (NMR) SPECTROSCOPY

All NMR spectra were attained using a Bruker DPX-300 (300 MHz) or DPX-400 (400 MHz) spectrometer. The deuterated solvents were used as supplied by Sigma-Aldrich. Chemical shifts obtained are recorded as δ values in parts per million (ppm) and are referenced to the solvent used. The following abbreviations are used in notation where appropriate:

s	Singlet
d	Doublet
t	Triplet
m	Mulitplet
br	Broad Peak

6.2.2 SIZE EXCLUSION CHROMATOGRAPHY (SEC)

SEC measurements were obtained using a Varian 390-LC-Multi detector suite equipped with a PL-AS RT/MT autosampler, PL-gel 3 μm guard column (50 x 7.5 mm), and two mixed-D columns (both 300 x 7.5 mm). Detection can occur using a differential refractive index, light scattering, and ultraviolet detectors. The flow rate was at 1 mL/min using a DMF solution as an eluent.

6.2.3 INFRARED SPECTROSCOPY

FT-IR (Fourier Transform-Infrared Spectroscopy) spectra were recorded, using a Bruker ALPHA FT-IR spectrometer, for each sample with an acquisition time of 1 hour. Increases in intensity of the OH stretch are key but changes in the peaks of the spectra at 2850-3000 cm^{-1} and 1350-1480 cm^{-1} were also noted and are due to the C-H stretches of the alkyl component seen for both pNIPAM and the alkane thiols. There

may also be new peaks between 1350 and 1700 cm^{-1} representing the amide of pNIPAM, however it is difficult to distinguish this from carboxyl groups that are found in the structure of GO.

6.2.4 THERMOGRAVIMETRIC ANALYSIS (TGA)

TGA was performed on each sample of grafted GO using a Mettler-Toledo TGA/DSC1 under a N2 atmosphere between 30-1000 °C, in order to observe any changes in the heat decomposition profile, and to monitor the removal of any grafted molecules.

6.2.5 ICE NUCLEATION ASSAY

The assay described is for one sample of grafted GO; the method was repeated for each sample of functionalised GO. A known mass of the grafted GO was suspended in Milli-Q water with the solution then subjected to sonication (20 minutes) to increase the dispersity and accuracy of concentration of the sample in water. 8 or 9 droplets (1 μL) were pipetted onto a glass slide covered with a hydrophobic barrier, ensuring that the droplets are clearly separated. The slide was placed inside a Linkham Scientific cryostage where it was cooled to -40 °C from 15°C at rate of 2 °C/minute, which allows for equilibrium before freezing temperatures are reached. The Ice nucleation process was observed through a Veho Discovery VMS-004 Deluxe USB microscope and Veho Microcapture software V 1.3. The experiment was repeated (at least) twice more using new droplets from the stock solution, recording a minimum of 24 freezing temperatures for each sample. The experimental set up is shown in Figure 33.

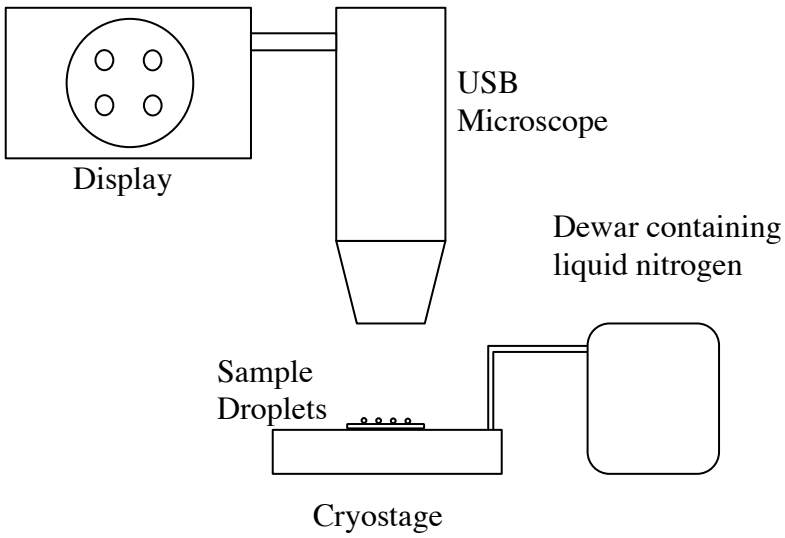

Figure 33 Experimental set up for recording ice nucleation values.

6.3 Synthesis of DMP RAFT agent

The 2-(dodecylthiocarbonothioylthio)-2-methylpropanoic acid (DMP) RAFT agent (Figure 34) was synthesized using the following procedure. Dodecanethiol (4.00 g, 4.73 mL, 19.76 mmol) was added drop wise to a stirred suspension of K_3PO_4 (4.20 g, 19.76 mmol) in acetone (60 mL) over a period of 25 minutes. CS_2 (4.10 g, 3.24 mL, 53.85 mmol) was added to the solution with an observed change in colour to bright yellow. The solution was stirred for 10 minutes, then 2-bromo-2-methylpropionic acid (3.00 g, 17.96 mmol) was added with a resultant KBr precipitate. After stirring for 16 hours, remove the solvent under reduced pressure and extract the residue into CH_2Cl_2 (2x200 mL) from 1M HCl (200 mL). The organic extracts were then washed with water (200 mL) and brine (200 mL) and dried over $MgSO_4$. The solvent was then removed under reduced pressure before purifying the residue via recrystallization in hexane.

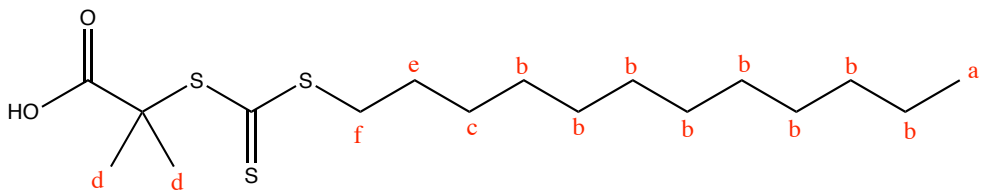

Figure 34 Molecular structure of 2-(dodecylthiocarbonothioylthio)-2-methylpropanoic acid with labelled hydrogen environments.

^{1}H NMR ($CDCl_3$) δ_{ppm}: 3.25-3.35 (2H, m, H^f); 1.90-2.00 (2H, m, H^e); 1.65-1.75 (6H, m, H^d); 1.50-1.65 (2H, m, H^c); 1.25-1.5 (16H, m, H^b); 0.8-0.9 (3H, t, H^a).

6.4 Polymerisation of N-isopropylacrylamide (NIPAM)

Two versions of pNIPAM (Figure 35) with differing molecular weights were synthesized using the following method. NIPAM (1.00 g, 8.84 mmol), 2-(dodecylthiocarbonothioylthio)-2-methylpropanoic acid (32.22 mg, 88.4 μmol), and 4,4'-azobis(4-cyanovaleric acid) (ACVA) (4.95 mg, 17.7 μmol) were all dissolved in methanol/toluene (1:1; 4 mL) in a glass vial containing a stirrer bar. The solution is in the ratio [monomer]:[chain transfer agent]:[initiator] = 100:1:0.2. This ratio can be adjusted to achieve different molecular weight polymers. A rubber septum was fitted to the vial, which was then degassed by bubbling with nitrogen gas for 30 minutes. The vial was then placed in an oil bath, previously heated to 70°C, for 35 minutes. After heating, the vial was submerged in liquid nitrogen to quench the polymerization. Solvent was then removed with compressed air. The solution was precipitated into diethyl ether (45 mL) and then re-precipitated and purified from THF into diethyl ether (45 mL). The product can then be purified 3 times by precipitation from toluene into diethyl ether, isolated centrifugation, and then dried under vacuum overnight with a resultant yellow solid.

To monitor the conversion rate of the polymerization, mesitylene (150 μL) is added previous to degassing with an aliquot taken for NMR analysis. Another aliquot is taken and analysed after quenching in liquid nitrogen. The decrease in intensity of the vinyl peaks associated with the monomer relative to mesitylene determines the overall monomer conversion.

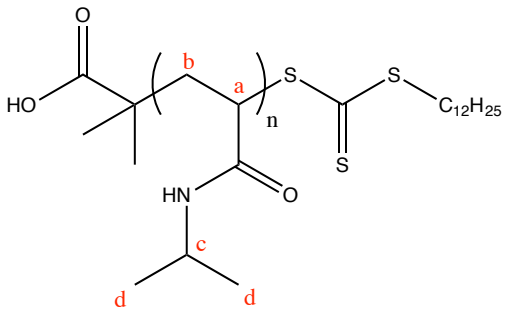

Figure 35 Molecular structure of pNIPAM with key hydrogen environments labelled.

$pNIPAM_{55}$: Conversion (NMR): 85%, M_n (SEC): 6200 $gmol^{-1}$, Dispersity (SEC): 1.08. **^{1}H NMR** ($CDCl_3$) δ_{ppm}: 3.90-4.10 (1H, br, H^a); 2.00-2.30 (2H, br, H^b); 1.45-1.90 (1H, br, H^c); 1.00-1.40 (6H, m, H^d).

$pNIPAM_{140}$: Conversion (NMR): 60.5%, M_n (SEC): 15700 $gmol^{-1}$, Dispersity (SEC): 1.11. **^{1}H NMR** ($CDCl_3$) δ_{ppm}: 3.90-4.15 (1H, br, H^a); 1.90-2.30 (2H, br, H^b); 1.50-1.70 (1H, br, H^c); 1.0-1.50 (6H, m, H^d).

6.5 GRAFTING THIOLS TO THE SURFACE OF GRAPHENE OXIDE

Grafting to the surface of GO can be achieved using standard Schlenk conditions under a nitrogen atmosphere. Methylamine (3 mL) was added to a solution of pNIPAM (20 mg) in DMF (3 mL) together with a catalytic amount of glacial ethanoic acid, generating effervescence. The mixture was then immediately transferred into a solution of bwGO (60 mg) in DMF (120 mL). The mixture of GO/pNIPAM was then heated to 50 °C for 1 hour, before being allowed to cool to room temperature and left to stir under nitrogen gas overnight (16 hours). The product is then collected via centrifugation (13200 rpm for 20 minutes), and was washed with water (30 minutes x 5) before being dried on a freeze dryer/under vacuum to remove excess water and leave a black solid.

The procedure was repeated for other samples replacing the DMF solvent with acetonitrile (3 mL) with the polymer and (120 mL) with the bwGO.

The polymer sample was interchanged in the method with a range of thiols, using the same quantities as stated, to vary the grafted molecule.

7. SAFETY CONSIDERATIONS

Particular precautions were required when dealing with thiols, as they are malodorous substances.

- A sulphide oxidizer solution was produced as stated in the 'Health and Safety in Laboratories' handbook. This was used to dispose of excess thiol and to clean all glassware and equipment that came into contact with the thiols.
- Bleach was used to further clean the glassware to ensure that any remaining odour was removed.

8. SUPPORTING INFORMATION

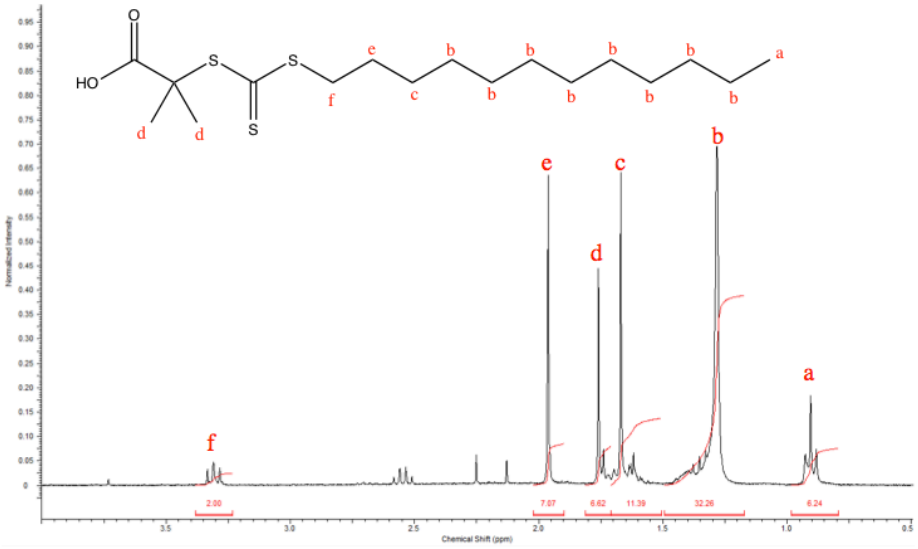

S 1 DMP NMR characterisation.

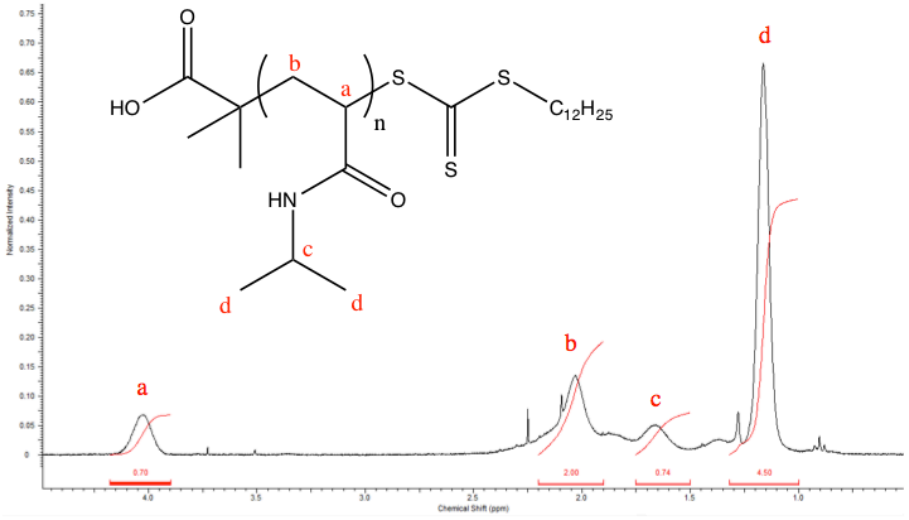

S 2 $pNIPAM_{140}$ NMR characterisation.

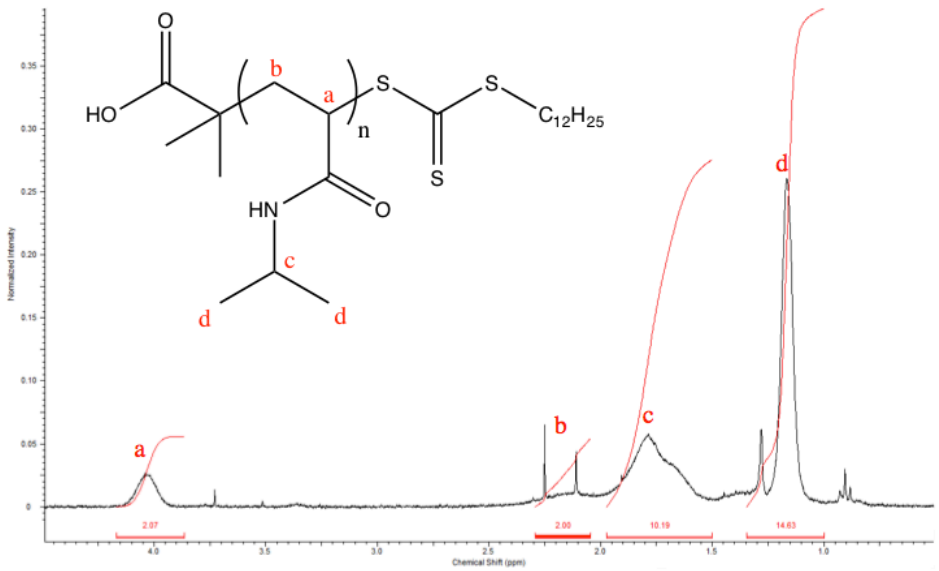

S 3 $pNIPAM_{55}$ NMR characterisation.

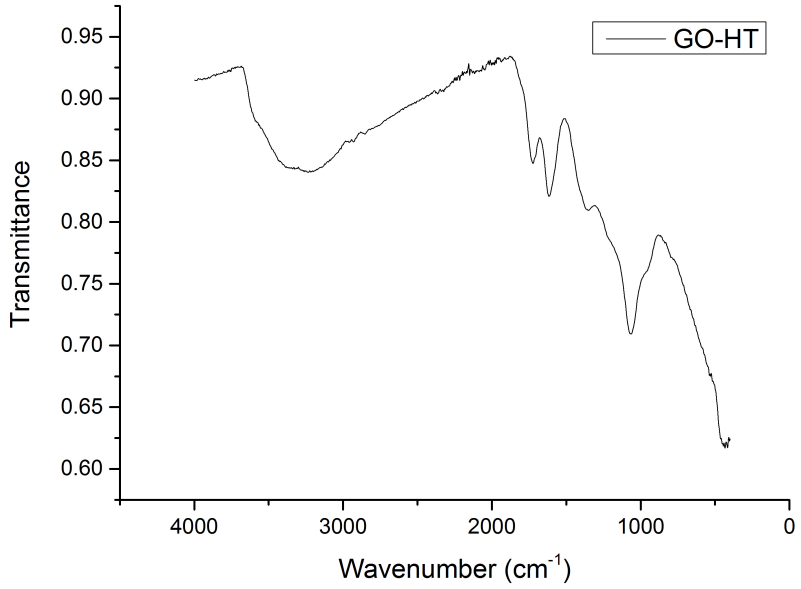

S 4 GO-HT IR spectrum.

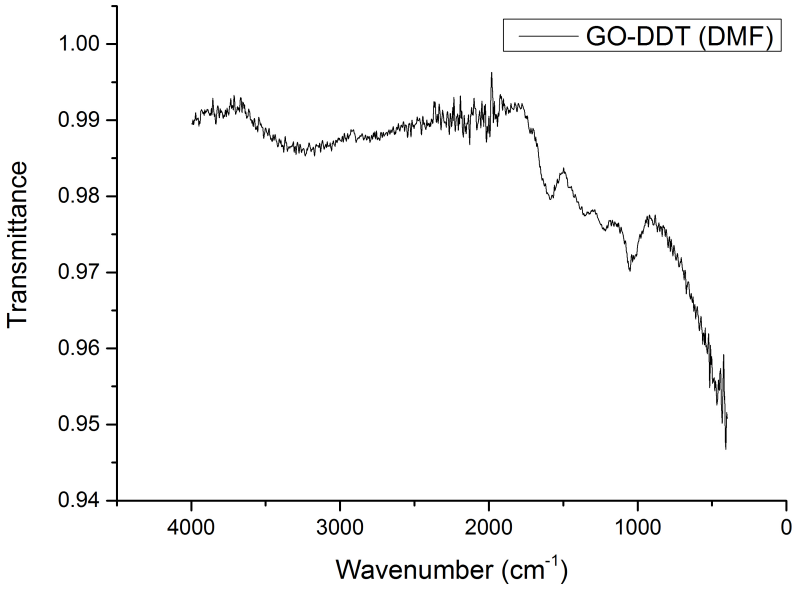

S 5 IR spectrum of GO-DDT using DMF as synthetic solvent.

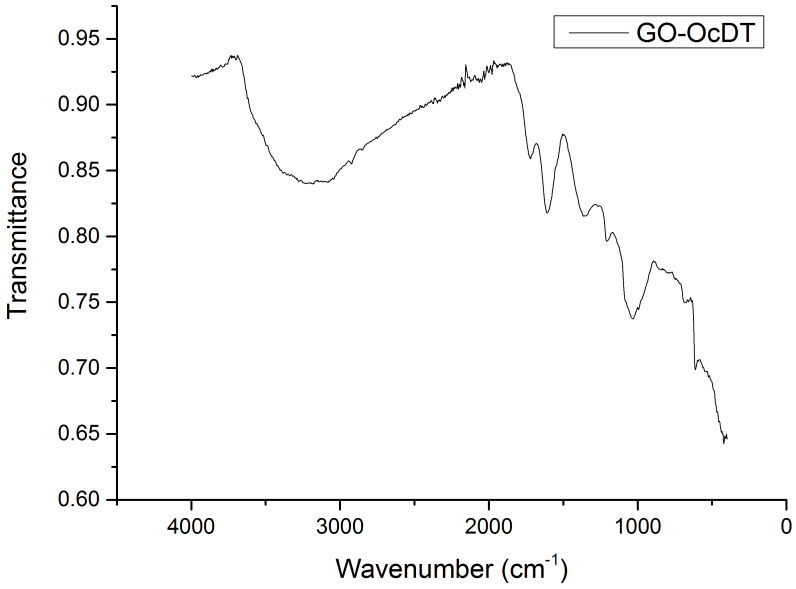

S 6 IR spectrum for GO-OcDT.

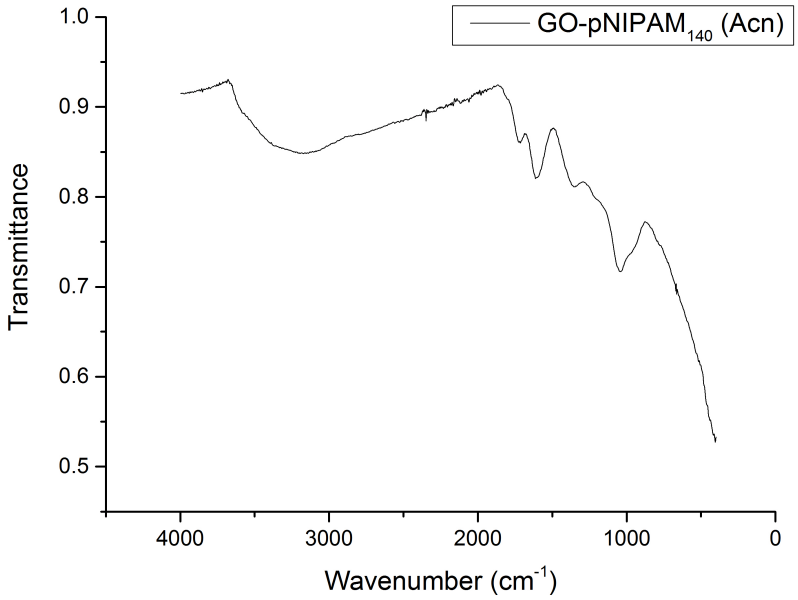

S 7 IR spectrum of GO-pNIPAM$_{140}$ using acetonitrile as the synthetic solvent.

9. REFERENCES

1 G. J. Christ, J. M. Saul, M. E. Furth and K.-E. Andersson, *Pharmacol. Rev.*, 2013, **65**, 1091–133.

2 J. L. Chaytor, J. M. Tokarew, L. K. Wu, M. Leclre, R. Y. Tam, C. J. Capicciotti, L. Guolla, E. Von Moos, C. S. Findlay, D. S. Allan and R. N. Ben, *Glycobiology*, 2012, **22**, 123–133.

3 H. C. Quevedo, K. E. Hatzistergos, B. N. Oskouei, G. S. Feigenbaum, J. E. Rodriguez, D. Valdes, P. M. Pattany, J. P. Zambrano, Q. Hu, I. Mcniece, A. W. Heldman and J. M. Hare, *Proc. Natl. Acad. Sci. U. S. A.*, 2009, **106**, 14022–7.

4 C. Mason and P. Dunnill, *Futur. Med.*, 2011, **18**, 243–245.

5 A. Fowler and M. Toner, *Ann. N. Y. Acad. Sci.*, 2005, **1066**, 119–135.

6 B. P. Best, *Rejuvenation Res.*, 2015, **18**, 422–436.

7 G. John Morris and E. Acton, *Cryobiology*, 2013, **66**, 85–92.

8 M. Moussa, F. Dumont, J. M. Perrier-Cornet and P. Gervais, *Biotechnol. Bioeng.*, 2008, **101**, 1245–1255.

9 M. M. Harding, P. I. Anderberg and A. D. J. Haymet, *Eur. J. Biochem.*, 2003, **270**, 1381–1392.

10 M. Griffith and M. W. F. Yaish, *Trends Plant Sci.*, 2004, **9**, 399–405.

11 C. J. Capicciotti, M. Leclere, F. A. Perras, D. L. Bryce, H. Paulin, J. Harden, Y. Liu and R. N. Ben, *Chem. Sci.*, 2012, **3**, 1408–1416.

12 M. I. Gibson, C. A. Barker, S. G. Spain, L. Albertin and N. R. Cameron, *Biomacromolecules*, 2009, **10**, 328–333.

13 J. A. Raymond and A. L. DeVries, *Proc. Natl. Acad. Sci. U. S. A.*, 1977, **74**, 2589–93.

14 A. J. Scotter, C. B. Marshall, L. A. Graham, J. A. Gilbert, C. P. Garnham and P. L. Davies, *Cryobiology*, 2006, **53**, 229–239.

15 M. I. Gibson, *Polym. Chem.*, 2010, **1**, 1141.

16 S. J. Cox, S. M. Kathmann, B. Slater and A. Michaelides, *J. Chem. Phys.*, 2015, **142**, 184704.

17 K. E. Zachariassen, E. Kristiansen, S. A. Pedersen and H. T. Hammel, *Cryobiology*, 2004, **48**, 309–321.

18 T. F. Whale, M. Rosillo-Lopez, B. J. Murray and C. G. Salzmann, *J. Phys. Chem. Lett.*, 2015, **6**, 3012–3016.

19 R. Cabriolu and T. Li, *Phys. Rev. E*, 2015, **91**, 1–7.

20 N. Du, X. Y. Liu and C. L. Hew, *J. Biol. Chem.*, 2003, **278**, 36000–36004.

21 H. L. F. Franks, J. Darlington, T. Schenz, S. F. Mathias, L. Slade, *Nature*, 1987, **325**, 146–148.

22 B. Wowk and G. M. Fahy, *Cryobiology*, 2002, **44**, 14–23.

23 T. Congdon, B. T. Dean, J. Kasperczak-Wright, C. I. Biggs, R. Notman and M. I. Gibson, *Biomacromolecules*, 2015, **16**, 2820–2826.

24 N. Hiranuma, O. Mohler, K. Yamashita, T. Tajiri, A. Saito, A. Kiselev, N. Hoffmann, C. Hoose, E. Jantsch, T. Koop and M. Murakami, *Nat. Geosci*, 2015, **8**, 273–277.

25 B. J. Murray, S. L. Broadley, T. W. Wilson, J. D. Atkinson and R. H. Wills, *Atmos. Chem. Phys.*, 2011, **11**, 4191–4207.

26 B. J. Murray, D. O'Sullivan, J. D. Atkinson and M. E. Webb, *Chem. Soc. Rev.*, 2012, **41**, 6519–54.

27 J. D. Atkinson, B. J. Murray, M. T. Woodhouse, T. F. Whale, K. J. Baustian, K. S. Carslaw, S. Dobbie, D. O'Sullivan and T. L. Malkin, *Nature*, 2013, **498**, 355–358.

28 M. Fitzner, G. C. Sosso, S. J. Cox and A. Michaelides, *J. Am. Chem. Soc.*, 2015, **137**, 13658–13669.

29 L. Lupi, A. Hudait and V. Molinero, *J. Am. Chem. Soc.*, 2014, **136**, 3156–3164.

30 A. Haji-Akbari and P. G. Debenedetti, *Proc. Natl. Acad. Sci.*, 2015, **112**, 10582–10588.

31 T. Inada, T. Koyama, F. Goto and T. Seto, *J. Phys. Chem. B*, 2012, **116**, 5364–5371.

32 J. Zhang, D. Jin, L. Zhao, X. Liu, J. Lian, G. Li and Z. Jiang, *Adv. Powder Technol.*, 2011, **22**, 613–616.

33 G. Fraux and J. P. K. Doye, *J. Chem. Phys.*, 2014, **141**, 1–2.

34 W. Gao, *Graphene Oxide Reduct. Recipes, Spectrosc. Appl.*, 2015, **39**, 228–240.

35 N. R. Wilson, P. a Pandey, R. Beanland, R. J. Young, I. a Kinloch, L. Gong, Z. Liu, K. Suenaga, J. P. Rourke, S. J. York and J. Sloan, *ACS Nano*, 2009, **3**, 2547–2556.

36 S. Pei and H.-M. Cheng, *Carbon N. Y.*, 2012, **50**, 3210–3228.

37 S. W. Chook, C. H. Chia, S. Zakaria, M. K. Ayob, K. L. Chee, N. M. Huang, H. M. Neoh, H. N. Lim, R. Jamal and R. Rahman, *Nanoscale Res. Lett.*, 2012, **7**, 541.

38 N. A. Zubir, C. Yacou, J. Motuzas, X. Zhang and J. C. Diniz da Costa, *Sci. Rep.*,

2014, **4**, 4594.

39 J. I. Paredes, A. Marti, J. M. D. Tasco and A. Martı, *Langmuir*, 2008, **24**, 10560–10564.

40 X. Zhao, L. Yang, X. Li, X. Jia, L. Liu, J. Zeng, J. Guo and P. Liu, *Bioconjug. Chem.*, 2015, **26**, 128–136.

41 P. Henrique, C. Camargo, K. G. Satyanarayana and F. Wypych, *Mater. Res.*, 2009, **12**, 1–39.

42 J. R. Potts, D. R. Dreyer, C. W. Bielawski and R. S. Ruoff, *Polymer (Guildf).*, 2011, **52**, 5–25.

43 H. R. Thomas, D. Phillips, N. Wilson, M. I. Gibson and J. P. Rourke, *Polym. Chem.*, 2015, **6**, 8270–8274.

44 S. Perrier and P. Takolpuckdee, *J. Polym. Sci. Part A Polym. Chem.*, 2005, **43**, 5347–5393.

45 G. Moad, Y. K. Chong, A. Postma, E. Rizzardo and S. H. Thang, *Polymer (Guildf).*, 2005, **46**, 8458–8468.

46 Y. Zheng, C. L. Su, J. Lu and K. P. Loh, *Angew. Commun.*, 2013, **52**, 8708–8712.

47 V. K. S. and H. R. M. Rashmi R Kokardekar*, *Internet J. Med. Updat.*, 2012, **7**, 60–63.

48 A. Gandhi, A. Paul, S. O. Sen and K. K. Sen, *Asian J. Pharm. Sci.*, 2015, **10**, 99–107.

49 R. Larciprete, S. Fabris, T. Sun, P. Lacovig, A. Baraldi and S. Lizzit, *J. Am. Chem. Soc.*, 2009, **133**, 17315–17321.

50 R. Larciprete, P. Lacovig, S. Gardonio, A. Baraldi and S. Lizzit, *J. Phys. Chem. C*, 2012, **116**, 9900–9908.

51 M. J. Mcallister, J. Li, D. H. Adamson, H. C. Schniepp, A. a Abdala, J. Liu, O. M. Herrera-alonso, D. L. Milius, R. Car, R. K. Prud and I. a Aksay, *Chem. Mater.*, 2007, **19**, 4396–4404.

52 M. Acik, G. Lee, C. Mattevi, A. Pirkle, R. M. Wallace, M. Chhowalla, K. Cho and Y. Chabal, *J. Phys. Chem. C*, 2011, **115**, 19761–19781.

53 S. Shi, L. Zhang, T. Wang, Q. Wang, Y. Gao and N. Wang, *Soft Matter*, 2013, **9**, 10966.

54 T. F. Whale, B. J. Murray, D. O'Sullivan, T. W. Wilson, N. S. Umo, K. J. Baustian, J. D. Atkinson, D. A. Workneh and G. J. Morris, *Atmos. Meas. Tech.*, 2015, **8**, 2437–2447.

55 N. K. S. Kirsten A. Koehler, Paul J. Demott, Sonjia M. Kreidenweis, Olga B. Popovicheva, Markus D. Petters, Christian M. Carrico, Elena D. Kiereeva, Tatiana D. Khokhlova, *Phys. Chem. Chem. Phys.*, 2009, **11**, 7906.

56 A. C. Zettlemoyer, N. Tcheurekdjian and C. L. Hosler, *ZAMP*, 1963, **14**, 496–502.

57 S. L. Broadley, B. J. Murray, R. J. Herbert, J. D. Atkinson, S. Dobbie, T. L. Malkin, E. Condliffe and L. Neve, *Atmos. Chem. Phys.*, 2012, **12**, 287–307.

58 D. a. Knopf and P. a. Alpert, *Faraday Discuss.*, 2013, **165**, 513.